Nonalcoholic fatty liver disease in CLOCK mutant mice

Xiaoyue Pan,[1,2] Joyce Queiroz,[1] and M. Mahmood Hussain[1,2,3]

[1]Department of Cell Biology, SUNY Downstate Medical Center, Brooklyn, New York, USA. [2]Department of Foundations of Medicine, NYU Long Island School of Medicine, Mineola, New York, USA. [3]VA New York Harbor Healthcare System, Brooklyn, New York, USA.

Nonalcoholic fatty liver disease (NAFLD) is becoming a major health issue as obesity increases around the world. We studied the effect of a circadian locomotor output cycles kaput (CLOCK) mutant ($Clk^{Δ19/Δ19}$) protein on hepatic lipid metabolism in C57BL/6 $Clk^{wt/wt}$ and apolipoprotein E–deficient ($Apoe^{-/-}$) mice. Both $Clk^{Δ19/Δ19}$ and $Clk^{Δ19/Δ19}$ $Apoe^{-/-}$ mice developed a full spectrum of liver diseases (steatosis, steatohepatitis, cirrhosis, and hepatocellular carcinoma) recognized in human NAFLD when challenged with a Western diet, lipopolysaccharide, or $CoCl_2$. We identified induction of CD36 and hypoxia-inducible factor 1α (HIF1α) proteins as contributing factors for NAFLD. Mechanistic studies showed that WT CLOCK protein interacted with the E-box enhancer elements in the promoters of the proline hydroxylase domain (PHD) proteins to increase expression. In $Clk^{Δ19/Δ19}$ mice, PHD levels were low, and HIF1α protein levels were increased. When its levels were high, HIF1α interacted with the $Cd36$ promoter to augment expression and enhance fatty acid uptake. Thus, these studies establish a regulatory link among circadian rhythms, hypoxia response, fatty acid uptake, and NAFLD. The mouse models described here may be useful for further mechanistic studies in the progression of liver diseases and in the discovery of drugs for the treatment of these disorders.

Introduction

Nonalcoholic fatty liver disease (NAFLD) encompasses a continuum of liver abnormalities, from fatty liver to steatohepatitis (NASH) with or without fibrosis, cirrhosis, and hepatocellular carcinoma (1–3). Although fatty liver is considered reversible and benign, recent studies indicate that it can advance to NASH and fibrosis (1–3). NASH can progress to cirrhosis and hepatocellular carcinoma (HCC) in many individuals. NAFLD is the most common liver disease in the Western world. The global estimated prevalence of NAFLD is approximately 25% and is expected to increase in the future along with increases in metabolic disorders, such as metabolic syndrome, obesity, and diabetes (1, 2). The pathogenesis of NAFLD has long been modeled on a 2-hit theory of lipid accumulation followed by induction of inflammation; however, according to the new multiple-hit theory, it is clear that the pathogenesis of this disease is more complex and that multiple molecular pathways independently contribute to NAFLD (3).

A primary cause of NAFLD is deregulation of fatty acid metabolism involving increased de novo lipogenesis and reduced β-oxidation. Derangements in several other metabolic pathways, such as bile acid fluxes, immune/inflammatory responses, autophagy, and host–gut microbiota interactions, also contribute to NAFLD pathogenesis (1–3). Many of these pathways of bile acid fluxes, autophagy, and inflammation show circadian rhythmicity. Other factors, such as microbiota and high-fat diets, affect circadian circuitry. Therefore, chronodisruption may play a role in liver steatosis (4, 5). Circadian rhythms are controlled by few core transcription factors: circadian locomotor output cycles kaput (CLOCK), brain and muscle aryl hydrocarbon receptor nuclear translocator–like 1 (BMAL1), periods (PER1–3), and cryptochromes (CRY1 and CRY2). Early studies in CLOCK mutant ($Clk^{Δ19/Δ19}$) mice expressing a dominant-negative CLOCK transcription factor with abnormal circadian rhythms showed that these mice develop steatosis (6); however, biochemical and molecular mechanisms were not explored.

Under hypoxic conditions, hypoxia-inducible factor 1α (HIF1α) orchestrates a major adaptive response (7–10). Under normoxic conditions, the HIF1α protein undergoes oxygen-dependent prolyl hydroxylation by proline hydroxylase domain proteins 1, 2, and 3 (PHD1, PHD2, and PHD3) and is degraded by proteasomes (8, 9, 11). Under hypoxic conditions, HIF1α does not undergo proline hydroxylation and is not degraded, so cellular HIF1α concentrations increase. HIF1α then heterodimerizes with HIF1β and interacts with hypoxia response elements in several target gene promoters to increase gene expression — promoting angiogenesis and glycolysis and preventing cell proliferation (7). HIF1α and HIF1β are structurally similar to CLOCK and BMAL1, and their recognition sequences are very similar (12, 13). Hypoxia signaling and circadian CLOCK reciprocally regulate each other under hypoxic conditions (12, 14). However, the role of HIF1α in normoxic condition is unknown.

Here, we studied the development of liver diseases in $Clk^{Δ19/Δ19}$ mice bred on C57BL/6 WT ($Clk^{wt/wt}$) and apolipoprotein E–deficient ($Apoe^{-/-}$) backgrounds to identify mechanisms that contribute to NAFLD. Our studies show that $Clk^{Δ19/Δ19}$ mice develop different liver diseases, from hepatosteatosis to HCC, when subjected to environmental insults. At the mechanistic level, we demonstrate that disruptions in circadian rhythms induce hypoxia response factors and fatty acid uptake contributing to the pathogenesis of NAFLD.

Results

Clk[ΔII9/ΔII9] mice develop steatosis and steatohepatitis with age on a chow diet when compared with *Clk*[wt/wt] mice. We previously showed that *Clk*[ΔII9/ΔII9] mice fed chow and Western diets produce more lipoproteins and have higher plasma triglycerides than *Clk*[wt/wt] control mice (15). Here, we studied changes in hepatic lipids in *Clk*[ΔII9/ΔII9] mice fed a chow diet and compared them with their *Clk*[wt/wt] siblings. *Clk*[ΔII9/ΔII9] mice gained more weight than controls with age (Supplemental Figure 1A; supplemental material available online with this article; https://doi.org/10.1172/JCI132765DS1). Oil Red O staining showed increased hepatosteatosis in *Clk*[ΔII9/ΔII9] mice compared with *Clk*[wt/wt] controls (Supplemental Figure 2A). Although hepatic triglyceride levels were not different in *Clk*[wt/wt] and *Clk*[ΔII9/ΔII9] mice at 1 or 3 months of age, *Clk*[ΔII9/ΔII9] mice on a chow diet accumulated more hepatic triglycerides than *Clk*[wt/wt] mice did at 6 and 10 months of age (Supplemental Figure 2B). Plasma alanine aminotransferase (ALT) levels were similar in *Clk*[wt/wt] and *Clk*[ΔII9/ΔII9] mice until 6 months; however, 10-month-old *Clk*[ΔII9/ΔII9] mice had significantly higher plasma ALT levels, indicating liver damage (Supplemental Figure 2C). Livers of 3- to 10-month-old *Clk*[ΔII9/ΔII9] mice took up more intraperitoneally injected (i.p.-injected) [³H]-labeled oleic acid (OA) than *Clk*[wt/wt] mice (Supplemental Figure 2D). These studies indicate that *Clk*[ΔII9/ΔII9] livers take up more fatty acids, accumulate higher amounts of triglycerides, and develop hepatosteatosis with age on chow diet.

To discover factors contributing to age-dependent changes in the livers of *Clk*[ΔII9/ΔII9] mice, we measured candidate genes involved in 4 different pathways: lipid metabolism, endoplasmic reticulum (ER) stress, inflammatory response, and cancer. Significant upregulation of genes involved in lipid uptake (*Cd36*), lipid synthesis (*Dgat2*, *Fas*, *Srebp1c*), and lipoprotein assembly (*Mttp*) and significant downregulation of genes involved in fatty acid oxidation (*Cpt1* and *Pparα*) were seen in 3-month-old *Clk*[ΔII9/ΔII9] versus *Clk*[wt/wt] mice (Supplemental Figure 2E). Fold changes in these genes were more prominent at 12 months. *Pparγ* and *Pgc1α* levels did not change. No significant changes were noted in the expression of genes in inflammatory response, ER stress, or cancer in 3-month-old *Clk*[ΔII9/ΔII9] mice (Supplemental Figure 2, F–H). However, significant changes were observed in the expression of genes involved in these pathways in 12-month-old *Clk*[ΔII9/ΔII9] mice (Supplemental Figure 2, F–H). At 12 months, expression of *Ire1α*, *Xbp1*, and *Atf4* increased, suggesting induction of ER stress. Increases in *Tnfα*, *Il6*, monocyte chemoattractant protein-1 (*Mcp1*), and *Cd68* mRNAs suggest macrophage infiltration and an inflammatory response. Increases in *Mdm2* and decreases in *Trp53* expression reflect increased susceptibility to carcinogenesis. These studies indicated that changes in lipid metabolism gene expression precede changes in other pathways in *Clk*[ΔII9/ΔII9] mice.

Accelerated hepatosteatosis in Clk[ΔII9/ΔII9] *mice fed cholate-containing high-fat and Western diets*. We then asked how different dietary insults affect the progression of hepatosteatosis. Male 3-month-old *Clk*[ΔII9/ΔII9] mice fed a cholate-containing high-fat diet for 2 months were leaner (Supplemental Figure 1B) and developed hepatomegaly and had grossly enlarged livers compared with *Clk*[wt/wt] mice (Supplemental Figure 2I, top). Macrovesicular steatohepatitis was evident in the livers of *Clk*[ΔII9/ΔII9] mice after Oil Red O staining (Supplemental Figure 2I, bottom). The liver/body weight ratio was significant-

ly higher in *Clk*[ΔII9/ΔII9] than in *Clk*[wt/wt] mice (Supplemental Figure 2J) because of increases in liver weights (not shown) and decreases in total body weights (Supplemental Figure 1B). Quantitative analyses revealed higher levels of triglyceride and thiobarbituric acid–reactive substances (TBARS), indicators of oxidized lipids, in the livers of *Clk*[ΔII9/ΔII9] mice (Supplemental Figure 2K). In addition, *Clk*[ΔII9/ΔII9] mice showed several-fold increases in plasma ALT and aspartate aminotransferase (AST) levels (Supplemental Figure 2L), indicating significant liver dysfunction. Livers of *Clk*[ΔII9/ΔII9] mice took up more i.p.-injected fatty acids (Supplemental Figure 2M). Hence, *Clk*[ΔII9/ΔII9] mice on a cholate-containing high-fat diet developed more hepatosteatosis in 2 months than did *Clk*[wt/wt] mice.

Next, 3-month-old male *Clk*[wt/wt] and *Clk*[ΔII9/ΔII9] mice were fed a high-cholesterol, high-fat Western diet for 2 months. *Clk*[ΔII9/ΔII9] mice were heavier (Supplemental Figure 1C), had higher amounts of hepatic triglyceride (Supplemental Figure 2N) and TBARS (Supplemental Figure 2O), and had increased plasma ALT levels (Supplemental Figure 2P) compared with *Clk*[wt/wt] controls. Macrovesicular steatohepatitis was evident after Oil Red O staining (Supplemental Figure 2Q). Further, *Clk*[ΔII9/ΔII9] mice took up more i.p.-injected [³H]OA (Supplemental Figure 2R). Ex vivo studies with liver slices showed increased fatty acid uptake and reduced fatty acid oxidation (Supplemental Figure 2S). Expression of genes in fatty acid uptake (*Cd36*), lipid synthesis (*Dgat2*, *Pparγ*), and lipoprotein secretion (*Mttp*) increased in *Clk*[ΔII9/ΔII9] compared with *Clk*[wt/wt] mice (Supplemental Figure 2T). Expression of *Pparα* and *Cpt1a*, involved in fatty acid oxidation, were decreased. Livers of *Clk*[ΔII9/ΔII9] mice had higher levels of mRNA involved in the inflammatory response. Analyses of ER stress response genes showed significant increases in *Ire1α*, *Xbp1*, and *Atf4* in *Clk*[ΔII9/ΔII9] mice. Genes involved in cancer progression were unaltered, except for some decrease in *Trp53*, in *Clk*[ΔII9/ΔII9] mice compared with controls. Thus, a Western diet induces steatosis, ER stress, and an inflammatory response but does not affect cancer genes in *Clk*[ΔII9/ΔII9] mice.

CLOCK regulates CD36 in liver-derived cells by regulating PHD proteins and HIF1α. The above studies indicated that the earliest response in chow-fed *Clk*[ΔII9/ΔII9] mice was upregulation of genes in lipid uptake, lipogenesis, and lipoprotein assembly (Supplemental Figure 2E). We previously elucidated mechanisms in the regulation of *Mttp* by CLOCK and BMAL1 (16, 17). Here, we concentrated on the mechanisms by which CLOCK regulates CD36. First, we hypothesized that upregulation of *Srebp1c* might be responsible for increased CD36 expression. Small interfering (si) CLOCK (*siClk*) in human hepatoma Huh7 cells and mouse primary hepatocytes had no effect on *Srebp1c* mRNA levels (Supplemental Figure 3, A and B). Furthermore, approximately 80% knockdown of *Srebp1c* had no effect on *Cd36* mRNA in Huh7 and primary mouse hepatocytes (Supplemental Figure 3, C and D). Thus, changes in *Cd36* mRNA are unrelated to changes in *Srebp1c* expression in *Clk*[ΔII9/ΔII9] mice. We previously showed that *Shp*, *Usf2*, and *Gata4* are involved in the regulation of *Mttp*, *Abca1*, and *Abcg5*/g8, respectively (15–17). Knockdown of these genes had no effect on *Cd36* mRNA (Supplemental Figure 3E). Therefore, we looked for other genes that might be involved in the regulation of CD36. Hypoxia and HIF1α regulate CD36 expression in macrophages and in corneal and retinal tissues (18–20). We asked whether HIF1α could regulate CD36 in liver-derived cells under normoxic conditions.
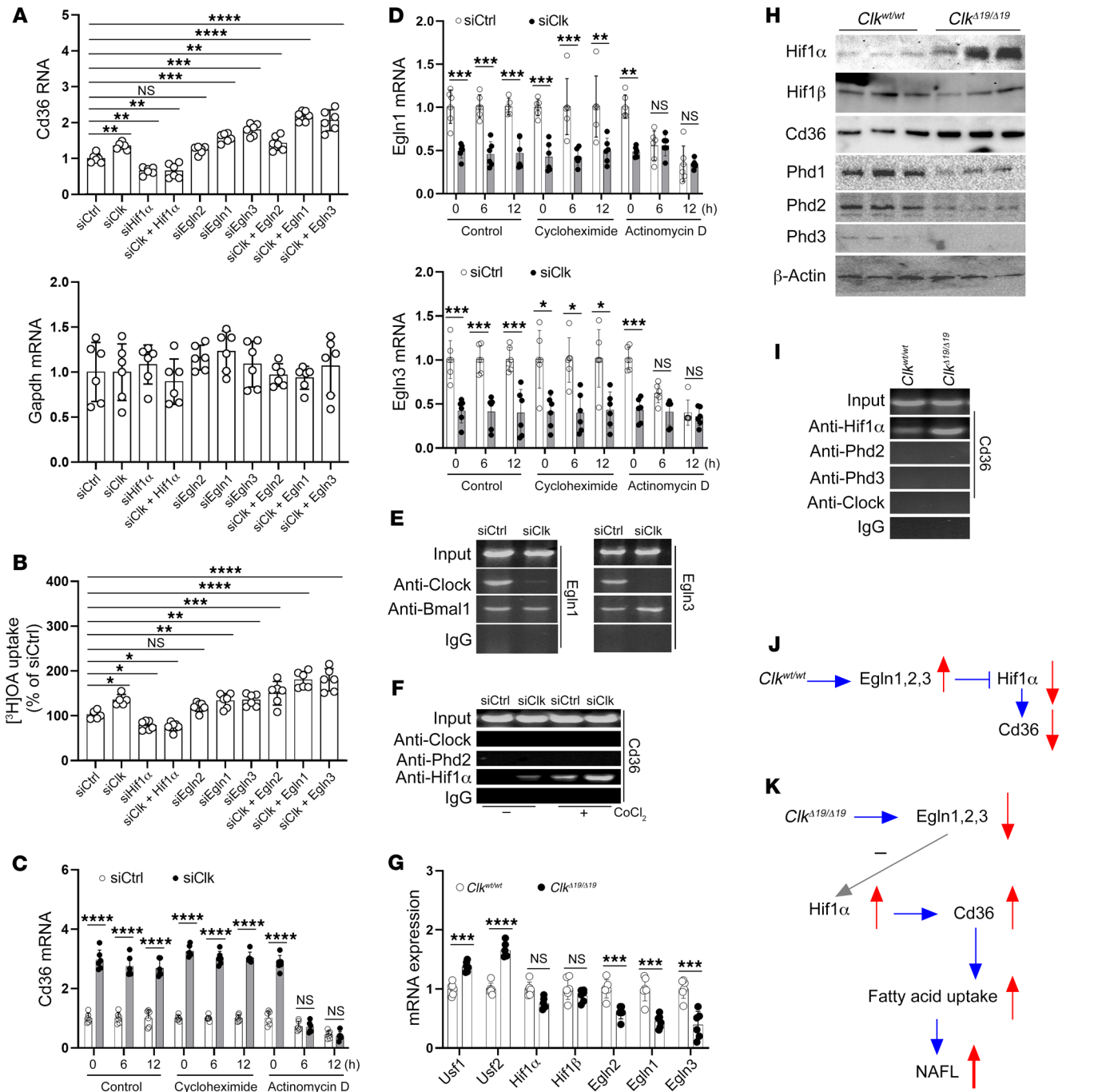
Figure 1. CLOCK regulates PHD proteins and HIF1α to regulate CD36. (**A–F**) Primary hepatocytes from WT chow-fed mice were used for these studies. (**A** and **B**) Hepatocytes were transfected in triplicate with indicated siRNAs, and *Cd36* (top) and *Gapdh* (bottom) mRNA levels were measured after 72 hours. (**B**) After 72 hours, cells were incubated with 0.5 μCi of [³H]OA. After 1 hour, cells were washed, and radioactivity was quantified. (**C** and **D**) Primary hepatocytes were transfected in triplicate with *siCtrl* or *siClk* for 72 hours and treated with cycloheximide (20 μM) or actinomycin D (2 μM) for 6 or 12 hours. *Cd36* (**C**) or *Egln2* and *Egln3* (**D**) mRNA levels were quantified. Data are representative of 3 experiments; mean ± SD; *P < 0.05, **P < 0.01, ***P < 0.001, ****P < 0.0001; multiple-comparisons 1-way ANOVA. (**E**) Hepatocytes were transfected with *siClk* or *siCtrl*. After 72 hours, ChIP was performed using indicated antibodies to amplify E-boxes (Supplemental Figure 5B) in *Egln1 and Egln3* promoters. Data are representative of 2 experiments. (**F**) Hepatocytes transfected with *siClk* or *siCtrl* for 48 hours were treated with or without CoCl₂ for 12 hours and used for ChIP to study the binding of HIF1α (Supplemental Figure 5C) in the *Cd36* promoter. Data are representative of 2 independent experiments. (**G** and **H**) Livers from chow-fed, male, 10-month-old *Clk^Δ19/Δ19* and *Clk^wt/wt* mice (*n* = 5 per group) were used to measure mRNA (**G**) (mean ± SD; ***P < 0.001, ****P < 0.0001, multiple *t* tests compared with controls; representative of 2 experiments) and protein levels (**H**). (**I**) Livers from chow-fed, male, 10-month-old *Clk^Δ19/Δ19* and *Clk^wt/wt* mice were used for ChIP; representative of 2 experiments. (**J** and **K**) Schematic diagram explaining the molecular mechanisms regulating CD36 expression and OA uptake in livers of *Clk^Δ19/Δ19* and *Clk^wt/wt* mice. (**J**) In *Clk^wt/wt* mice, CLOCK binds to the E-boxes in the promoters of *Phd* genes to increase transcription and protein levels. In the presence of high PHD levels, HIF1α protein is degraded. (**K**) In *Clk^Δ19/Δ19* mice, expression of PHD proteins is low and HIF1α protein levels are increased. Under these conditions, HIF1α binds to the *Cd36* promoter to increase transcription and protein levels. This might be one mechanism for increased fatty acid uptake in these mice.

siClk increased, but *siHif1α* reduced, *Cd36* mRNA levels in mouse primary hepatocytes (Figure 1A) and in human hepatoma Huh7 cells (Supplemental Figure 4A) without affecting *Gapdh* mRNA levels. Further, *siClk* was unable to increase *Cd36* in the presence of *siHif1α*, suggesting involvement of HIF1α in the regulation of CD36 by CLOCK (Figure 1A and Supplemental Figure 4A). HIF1α protein levels are regulated by PHD proteins (10, 11). Knockdown of PHD1 (*Egln2*), PHD2 (*Egln1*), and PHD3 (*Egln3*) increased *Cd36* expression in hepatocytes and Huh7 cells (Figure 1A and Supplemental Figure 4A). *siEgln1* and *siEgln3* combined with *siClk* increased *Cd36* expression more than individual siRNA, indicating additive effects (Figure 1A and Supplemental Figure 4A). These changes in *Cd36* mRNA levels correlated with increases and decreases in the uptake of OA in these cells (Figure 1B and Supplemental Figure 4B). These studies suggest that HIF1α as well as PHD2 and PHD3 proteins might be involved in the regulation of CD36 and fatty acid uptake by CLOCK. We further studied the regulation of HIF1α and PHD proteins by overexpressing *CLOCK* in Huh7 cells (Supplemental Figure 4, C and D). CLOCK overexpression reduced OA uptake in Huh7 cells and increased mRNA levels of *EGLN2*, *EGLN1*, and *EGLN3* but had no effect on *HIF1α* mRNA levels (Supplemental Figure 4D). These studies indicated that CLOCK increases *EGLN* mRNA levels and decreases hepatic fatty acid uptake.

Attempts were then made to understand transcriptional and translational mechanisms in the upregulation of HIF1α and CD36 by CLOCK. Increases in *Cd36* mRNA levels by *siClk* were unaffected by cycloheximide, a protein synthesis inhibitor, but were abrogated in the presence of actinomycin D, an inhibitor of transcription, at 6 and 12 hours compared with 0 hour (Figure 1C), indicating transcriptional activation. Unlike *Cd36*, *Egln1* and *Egln3* mRNA levels were lower in *siClk*-treated cells (Figure 1D). These levels were unaffected by cycloheximide. However, *Egln1* and *Egln3* mRNA levels were reduced in siControl-treated (siCtrl-treated) cells after actinomycin D treatment, indicating that *Egln1* and *Egln3* gene transcription is high in control cells compared with *siClk*-treated cells because of increased transcription. Thus, CLOCK may interact with *Egln1* and *Egln3* gene promoters to increase their transcription. To test this, we looked for potential enhancer boxes (E-boxes) in the *Egln1* and *Egln3* promoters (Supplemental Figure 5). Human (Supplemental Figure 5A) and mouse (Supplemental Figure 5B) *Egln1* and *Egln3* promoters contain 1 to 3 E-boxes. To test whether CLOCK binds to any of these boxes, we performed chromatin immunoprecipitation (ChIP) assays and observed that both CLOCK and BMAL1 interact with *Egln1* and *Egln3* promoters in siCtrl-treated cells (Figure 1E). Binding of CLOCK to *Egln* promoters has been reported in genome-wide transcriptomic analysis (21). In our study, binding of CLOCK was abrogated in *siClk*-treated cells (Figure 1E). Surprisingly, BMAL1 binding was not reduced in *siClk*-treated cells, perhaps because BMAL1 binds to these sites, and CLOCK may interact with already-bound BMAL1 to increase transcription.

We next studied the binding of CLOCK, PHD2, and HIF1α proteins to the *Cd36* promoter; binding was undetectable in *siCtrl*-treated hepatocytes (Figure 1F). However, binding of HIF1α to the *Cd36* promoter was increased in *siClk*-treated cells (Figure 1F). Cobalt chloride (CoCl$_2$), an activator of HIF1α (7), increased the

binding of HIF1α to the *Cd36* promoter in *siCtrl*- and *siClk*-transfected cells (Figure 1F). Thus, it is likely that CLOCK deficiency increases HIF1α binding to the *Cd36* promoter and that CoCl$_2$ enhances this binding. This may increase CD36 protein, uptake of fatty acids, and lipid synthesis, contributing to steatosis.

Next, we asked whether these mechanisms are operative in *Clk^{Δ19/Δ19}* mice. *Egln2*, *Egln1*, *Egln3*, and *Hif1α* mRNA levels showed circadian rhythms in *Clk^{wt/wt}* mice but not in *Clk^{Δ19/Δ19}* mice (Supplemental Figure 6). Circadian rhythms for *Egln* mRNAs were not in databases (22, 23), but *Hif1α* changes were similar to those reported in circadian rhythm gene databases (23). *Clk^{Δ19/Δ19}* livers had lower *Egln1*, *Egln2*, and *Egln3* mRNA and protein levels compared with *Clk^{wt/wt}* controls (Figure 1, G and H). Although mRNA levels of *Hif1α* were not different (Figure 1G), HIF1α protein levels were significantly higher in *Clk^{Δ19/Δ19}* than in *Clk^{wt/wt}* hepatocytes (Figure 1H). Similarly, CD36 protein levels were higher in *Clk^{Δ19/Δ19}* livers (Figure 1H). ChIP assays showed that higher amounts of HIF1α were associated with the *Cd36* promoter in *Clk^{Δ19/Δ19}* mice (Figure 1I). These studies indicated that *Clk^{Δ19/Δ19}* livers had reduced levels of *Egln* mRNA but had higher levels of HIF1α and CD36 proteins and that there was increased binding of HIF1α to the *Cd36* promoter. Based on these data, we propose that CLOCK interacts with E-boxes in the *Egln* promoters to increase PHD expression. When PHD proteins are high, HIF1α levels are reduced, and binding of HIF1α to the *Cd36* promoter is reduced (Figure 1J). In *Clk^{Δ19/Δ19}* mice, the expression of PHD proteins is reduced, HIF1α protein levels are increased, and binding of HIF1α to the *Cd36* promoter is enhanced (Figure 1K). This may augment CD36 protein and uptake of fatty acids by the liver, which could contribute to steatosis.

Role of HIF1α in hepatosteatosis in chow diet–fed Clk^{Δ19/Δ19} mice. To further investigate whether HIF1α plays a role in hepatosteatosis, we treated Western diet–fed *Clk^{Δ19/Δ19}* and *Clk^{wt/wt}* mice with CoCl$_2$, a known inducer of HIF1α activity (7). CoCl$_2$-treated *Clk^{Δ19/Δ19}* mice showed significantly reduced hepatic *Egln1* and *Egln3* mRNA levels compared with CoCl$_2$-treated *Clk^{wt/wt}* mice (Figure 2A). Although mRNA levels of *Hif1α* did not change, mRNA levels of its target gene *Vegf* (24, 25) increased significantly in *Clk^{Δ19/Δ19}* mice (Figure 2A). CoCl$_2$ treatment increased *Cd36*, *Acc*, *Fas*, and *Srebp1c* but decreased *Mttp*, *Cpt1*, and *Pparα* mRNA levels in *Clk^{Δ19/Δ19}* mice compared with controls (Figure 2B). CoCl$_2$ treatment increased all inflammatory markers measured except *Tlr2* (Figure 2C); enhanced ER stress markers *Ire1α*, *Xbp1*, and *Bip* without affecting *Atf4* and *Chop* (Figure 2D); and augmented cancer markers *Mdm2*, *Bcl2*, and *Bax* while decreasing *Trp53* in *Clk^{Δ19/Δ19}* mice compared with controls (Figure 2E). Oil Red O and anti-macrophage staining showed increased lipid droplets and macrophage content, respectively, in the livers of *Clk^{Δ19/Δ19}* mice treated with CoCl$_2$ compared with *Clk^{wt/wt}* mice (Figure 2F). CoCl$_2$ increased hepatic triglyceride (Figure 2G) and TBARS (Figure 2H) in *Clk^{Δ19/Δ19}* mice compared with controls. Plasma of these mice had higher ALT levels and reduced levels of β-hydroxybutyrate (β-HB) (Figure 2I). CoCl$_2$ increased OA uptake by the liver in vivo (Figure 2J), in liver slices (Figure 2K), and in isolated hepatocytes (Figure 2M) of *Clk^{Δ19/Δ19}* mice compared with controls. Fatty acid oxidation was reduced more in liver slices from *Clk^{Δ19/Δ19}* mice (Figure 2L). Furthermore, increased fatty acid uptake and reduced β-oxidation were seen in *Clk^{Δ19/Δ19}* hepatocytes (Figure 2N) treated with dimethyloxalylgly-
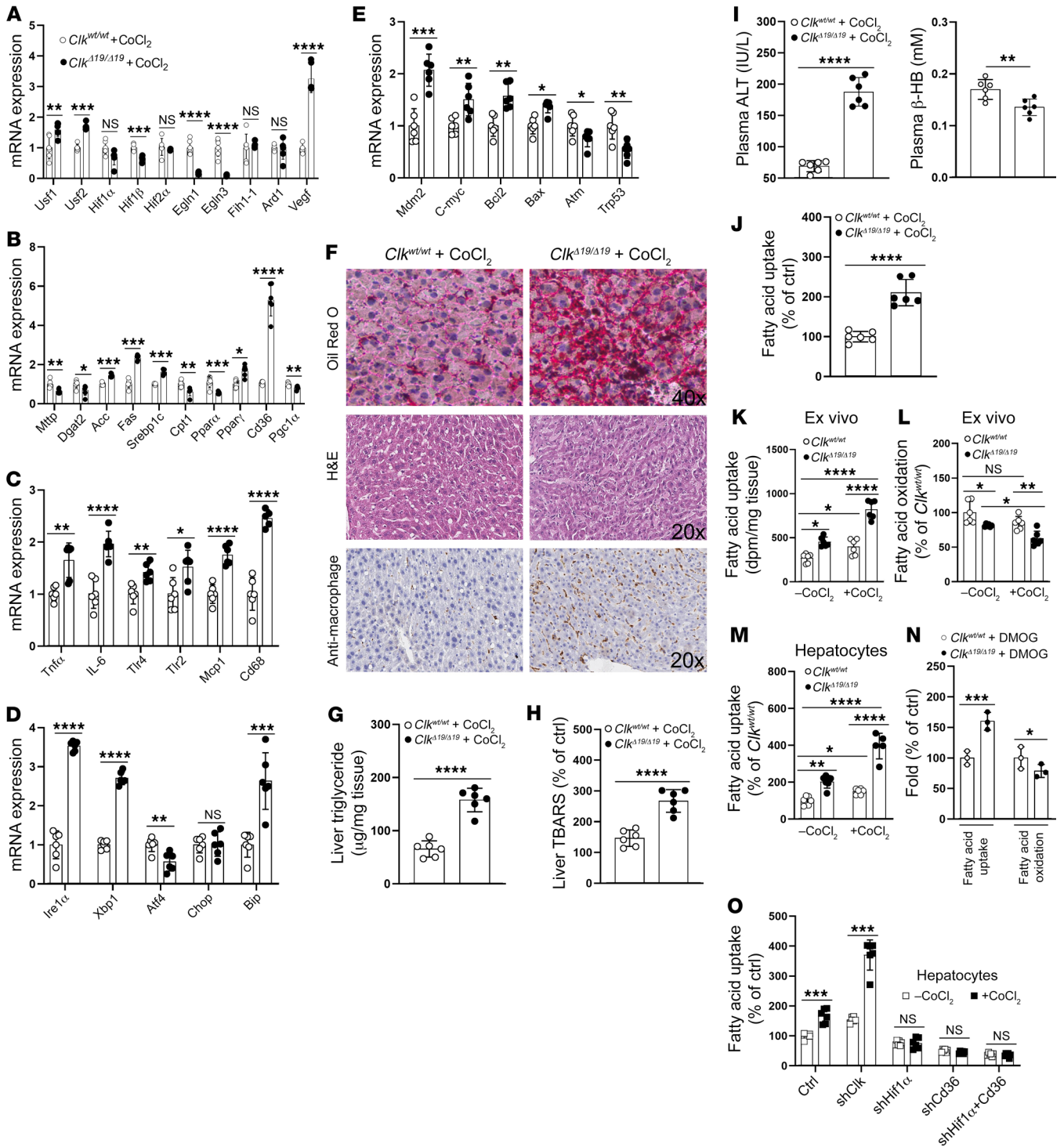
Figure 2. Hepatosteatosis in *Clk^{Δ19/Δ19}* mice challenged with CoCl₂. Male (8-month-old) *Clk^{Δ19/Δ19}* and *Clk^{wt/wt}* mice fed a Western diet for 2 months were injected i.p. 3 times with 30 mg/kg CoCl₂ on alternate days, and continued on the same diet ad libitum for 2 months. Mice were used for tissue analysis (*n* = 6 per group) or to study hepatic uptake of [³H]OA (*n* = 5–6 per group). (**A**–**E**) Livers were used to measure mRNA levels. Mean ± SD; *P < 0.05, **P < 0.01, ***P < 0.001, ****P < 0.0001, multiple *t* tests. (**F**) Frozen liver sections were used for Oil Red O, H&E, and anti-macrophage (anti-CD68) staining. Pictures are representative of 3 experiments. (**G** and **H**) Livers were used to measure triglyceride (**G**) and TBARS (**H**). Mean ± SD; ****P < 0.0001, Welch's 2-tailed *t* test. (**I**) Plasma ALT and β-HB levels in *Clk^{Δ19/Δ19}* mice injected with CoCl₂. Mean ± SD; **P < 0.01, ****P < 0.0001, Welch's 2-tailed *t* test. (**J**) *Clk^{Δ19/Δ19}* and *Clk^{wt/wt}* mice were injected with CoCl₂. Two weeks later, mice were injected i.p. with [³H]OA. After 2 hours, livers were collected, and radioactivity was measured. Mean ± SD; ****P < 0.0001, Welch's 2-tailed *t* test. (**K**) Liver slices from 10-month-old *Clk^{Δ19/Δ19}* and *Clk^{wt/wt}* mice treated with CoCl₂ were incubated with [³H]OA (1 μCi/mL) for 1 hour, washed, and used to measure protein and radioactivity. Mean ± SD; *P < 0.05, ****P < 0.0001, 2-way ANOVA, Šidák's multiple-comparisons test. (**L**) Liver slices from 10-month-old *Clk^{Δ19/Δ19}* and *Clk^{wt/wt}* mice treated with or without CoCl₂ were incubated with [¹⁴C]palmitic acid (PA) (1 μCi/mL) for 2 hours. ¹⁴CO₂ adsorbed to paper and acid-precipitated intermediates were counted. Mean ± SD; *P < 0.05, **P < 0.01, 2-way ANOVA, Šidák's multiple-comparisons test. (**M**) Primary hepatocytes from *Clk^{Δ19/Δ19}* and *Clk^{wt/wt}* mice were treated with CoCl₂ (250 μM) for 12 hours, incubated with 0.5 μCi/mL of [³H]OA for 1 hour, washed, and counted. Mean ± SD; *P < 0.05, **P < 0.01, ****P < 0.0001, 2-way ANOVA, Šidák's multiple-comparisons test. (**N**) Primary hepatocytes from *Clk^{Δ19/Δ19}* and *Clk^{wt/wt}* mice were treated with DMOG (500 μM) for 8 hours, incubated for 1 hour with 0.5 μCi/mL [³H]OA, and washed, and radioactivity was determined to measure uptake or hepatocytes were incubated with [¹⁴C]PA for 1 hour to study fatty acid oxidation. Mean ± SD; *P < 0.05, ***P < 0.001, 2-way ANOVA, Šidák's multiple-comparisons test. (**O**) WT hepatocytes were transduced in triplicate with adenoviruses expressing shCLOCK, shHIF1α, shCD36, or shCTRL. After 60 hours, cells were treated with CoCl₂ for 12 hours and fatty acid uptake was measured. Mean ± SD; ***P < 0.001, 2-way ANOVA, Šidák's multiple-comparisons test.

cine (DMOG), another activator of HIF1α (26). Similar studies in Huh7 cells transfected with *siClk* and treated with CoCl₂ or DMOG showed increased fatty acid uptake but reduced fatty acid oxidation in Huh7 cells (Supplemental Figure 7). Thus, activation of HIF1α increases uptake of fatty acids but decreases their oxidation in CLOCK-deficient cells compared with control cells.

To assess whether increased uptake of fatty acids by the liver was due to upregulation of HIF1α and CD36, isolated primary hepatocytes were transduced with adenoviruses expressing short hairpin (sh) *shClk*, *shHif1α*, or *shCd36* and were treated with CoCl₂ (Figure 2O). CoCl₂ treatment increased fatty acid uptake in control and *shClk*-treated hepatocytes. However, cells exposed to *shHif1α*, *shCd36*, and both *shHif1α* and *shCd36* did not show increased fatty acid uptake after CoCl₂ treatment. These studies suggested that HIF1α and CD36 participate in increased fatty acid uptake induced by CoCl₂.

The above studies identified HIF1α as a transcription factor involved in the upregulation of CD36 and in the induction of hepatosteatosis in *Clk^{Δ19/Δ19}* mice. We hypothesized that knockdown of HIF1α may prevent development of steatosis and hepatosteatosis in *Clk^{Δ19/Δ19}* mice. Injection of *shHif1α* in chow-fed *Clk^{Δ19/Δ19}* mice significantly reduced expression of *Hif1α* and levels of its target *Vegf* (Figure 3A) and reduced *Cd36* mRNA (Figure 3A) and protein (Figure 3A, inset) levels. Livers of *Clk^{Δ19/Δ19}* mice transduced with

shHif1α took up less fatty acid (Figure 3B). These mice had lower levels of hepatic TBARS, triglyceride, and cholesterol (Figure 3C), lower levels of plasma ALT and triglyceride, and normal levels of plasma cholesterol and β-HB (Figure 3D). Histologic studies showed reduced lipid staining, hepatocyte ballooning, macrophage infiltration, and HIF1α protein expression in *shHif1α*-recipient mice (Figure 3E). Transmission electron microscopy showed fewer lipid droplets in the livers of *shHif1α*-recipient *Clk^{Δ19/Δ19}* mice (Figure 3F). Expression analyses revealed reduced mRNA levels of lipogenesis and inflammatory response genes (Figure 3G). *shHif1α* had no effect on ER stress or cancer gene expression. These studies indicated that reduced HIF1α expression decreases the expression of genes in steatosis and inflammation and may help ameliorate steatohepatitis.

Hepatosteatosis and cirrhosis in Clk^{Δ19/Δ19} mice challenged with lipopolysaccharide. Next, we asked how Western diet–fed *Clk^{Δ19/Δ19}* male (Figure 4) and female (Supplemental Figure 8) mice would respond to a lipopolysaccharide (LPS) challenge that is known to induce an inflammatory response. LPS-injected *Clk^{Δ19/Δ19}* mice developed hepatomegaly and micronodular cirrhosis (Figure 4A). Livers from these mice showed increased Oil Red O (Figure 4B and Supplemental Figure 8A) and anti-macrophage staining (Figure 4B) compared with *Clk^{wt/wt}* mice. *Clk^{Δ19/Δ19}* livers had significantly higher amounts of triglyceride, cholesterol (Figure 4C and Supplemental Figure 8B), and TBARS (Figure 4D and Supplemental Figure 8C). These mice contained significantly more ALT but reduced levels of β-HB (Figure 4E and Supplemental Figure 8D). *Clk^{Δ19/Δ19}* livers took up more i.p.-injected OA (Figure 5A and Supplemental Figure 8E). Fatty acid oxidation was reduced (Figure 5B and Supplemental Figure 8E). Livers of *Clk^{Δ19/Δ19}* mice showed increased expression of the inflammatory response (Figure 5C and Supplemental Figure 8F) and ER stress genes (Figure 5D and Supplemental Figure 8G). There were modest increases in *Mdm2* and *C-myc* and reductions in *Trp53*, indicating changes favoring cancer in *Clk^{Δ19/Δ19}* mice (Figure 5E and Supplemental Figure 8H). Expression analyses also revealed induction of genes involved in lipogenesis and lipoprotein assembly as well as suppression of fatty acid oxidation (Figure 5F and Supplemental Figure 8I). Further, there were significant reductions in *Egln2*, *Egln1*, and *Egln3* mRNA levels (Figure 5G and Supplemental Figure 8J). Thus, LPS increases steatosis, ER stress, and inflammatory response in *Clk^{Δ19/Δ19}* mice, suggesting that these factors may promote cirrhosis.

LPS-treated *Clk^{Δ19/Δ19}* mice had significantly lower levels of hepatic *Egln2*, *Egln1*, and *Egln3* mRNA levels (Figure 5G). There was no change in *Hif1α* mRNA levels compared with controls. We also studied the effects of CLOCK knockdown and LPS treatment in human hepatoma Huh7 cells (Figure 5H). *siClk* reduced the mRNA level of *EGLN2*, *EGLN1*, and *EGLN3* and *HIF1β* but had no effect on *HIF1α* and *GAPDH* (Figure 5H), and this response was considerably enhanced after LPS treatment. Next, we looked at changes in protein levels. HIF1α and CD36 protein levels increased in LPS-treated *Clk^{Δ19/Δ19}* mice compared with controls (Supplemental Figure 8K). *siClk* increased CD36 and HIF1α protein levels in Huh7 cells, and these protein levels increased more after LPS treatment (Figure 5I). *siClk* reduced PHD1 and PHD2 protein levels; LPS further reduced these protein levels (Figure 5I). Further, the binding of HIF1α to the *Cd36* promoter was high
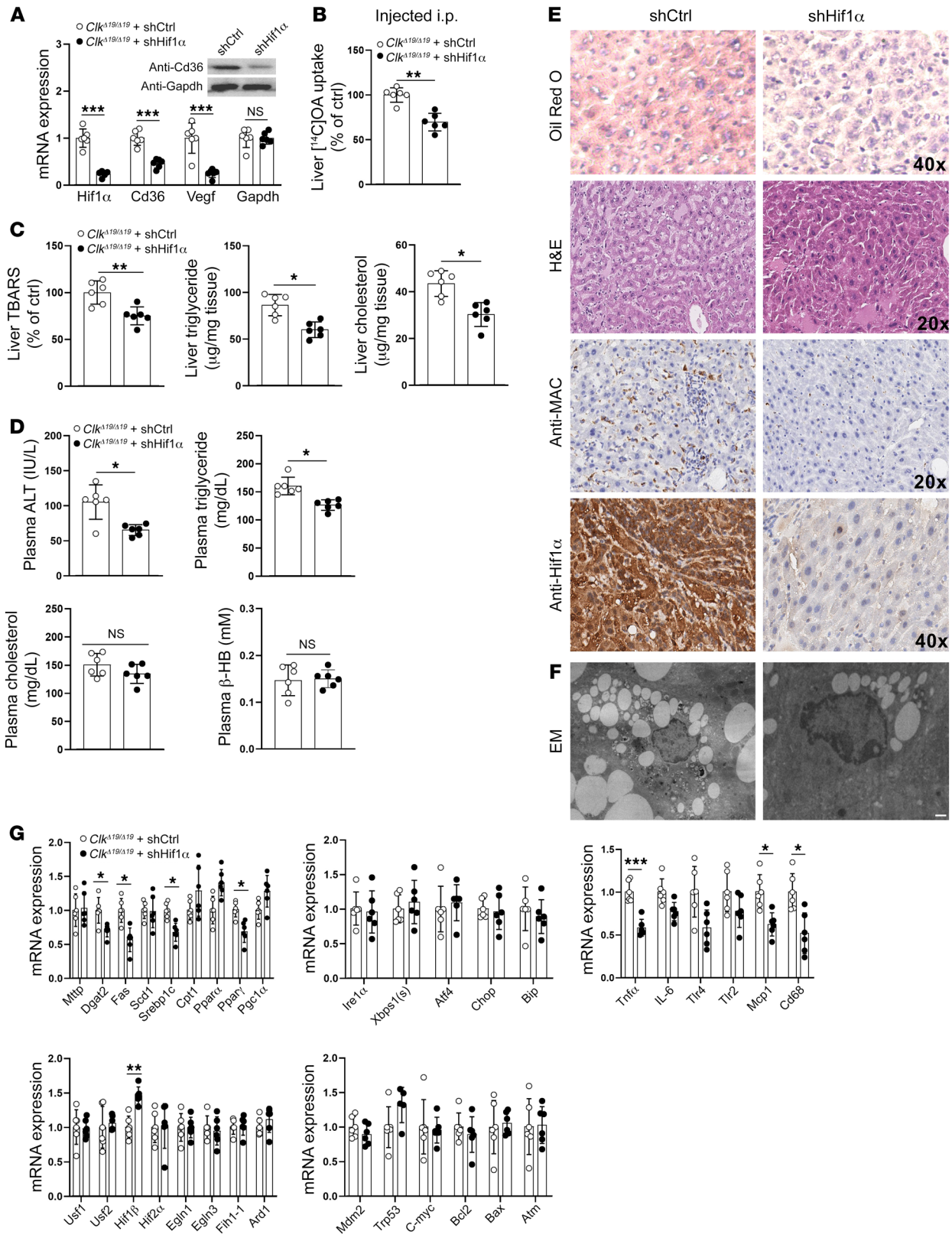
Figure 3. Decreased hepatosteatosis after knockdown of HIF1α in *Clk^{Δ19/Δ19}* mice. *Clk^{Δ19/Δ19}* mice (male, 10 months old, chow-fed, 5–6 per group) were injected once via tail vein with lentiviruses expressing either shCtrl or shHIF1α (1 × 10^9 PFU/mouse). After 2 weeks, plasma and livers were collected. Another set of animals was used for fatty acid uptake studies (*n* = 3 per group). (**A**) Liver samples were used to measure *Hif1α*, *Cd36*, *Vegf*, and *Gapdh* mRNA and protein levels of CD36 and Gapdh (inset). Mean ± SD; ***P < 0.001, multiple *t* tests. (**B**) For hepatic fatty acid uptake, mice were injected i.p. with 1.0 μCi/mouse of [^3H]OA. After 2 hours, livers were collected to measure radioactivity. Mean ± SD; **P < 0.0001, Welch's 2-tailed *t* test. (**C**) Liver triglyceride, cholesterol, and TBARS levels were lower in *Clk^{Δ19/Δ19}* mice 2 weeks after injection of *shHif1α*. Mean ± SD; *P < 0.01, **P < 0.001, Welch's 2-tailed *t* test. (**D**) Plasma ALT and triglyceride levels were reduced in *shHif1α*-injected *Clk^{Δ19/Δ19}* mice, but plasma cholesterol and β-HB concentrations were normal. Mean ± SD; *P < 0.001, Welch's 2-tailed *t* test. (**E**) Liver sections were stained with Oil Red O, H&E, and anti-macrophage and anti-HIF1α antibodies. Data are representative of 2 experiments. (**F**) Transmission electron microscopy (EM) revealed reduced lipid droplets in *Clk^{Δ19/Δ19}* mice injected with *shHif1α* (scale bar: 100 μm). (**G**) Quantification of different mRNAs in livers of *Clk^{Δ19/Δ19}* mice 2 weeks after injection of shHIF1α. Mean ± SD; *P < 0.05, **P < 0.01, ***P < 0.001, multiple *t* tests.

in *Clk^{Δ19/Δ19}* mice. This binding increased in LPS-injected mice (Figure 5J). These studies indicated that an inflammatory insult augments HIF1α and CD36 proteins in *Clk^{Δ19/Δ19}* mice. Thus, normal CLOCK activity may reduce an LPS-induced inflammatory response in *Clk^{wt/wt}* mice.

Clk^{Δ19/Δ19} Apoe^{−/−} mice develop steatohepatitis and cirrhosis with age on chow diet. We showed that *Clk^{Δ19/Δ19} Apoe^{−/−}* mice develop more robust atherosclerosis than *Apoe^{−/−}* mice (15). Here, we studied changes in the livers of *Clk^{Δ19/Δ19} Apoe^{−/−}* mice fed a chow diet and compared them with livers of control *Apoe^{−/−}* mice. *Apoe^{−/−}* mice do not develop liver diseases on chow diet; however, they do develop steatosis, NASH, and fibrosis when fed different diets (27, 28). To avoid the effects of Western diet, *Clk^{Δ19/Δ19} Apoe^{−/−}* mice were fed only a chow diet, and development of NAFLD was compared against *Apoe^{−/−}* mice. Hepatic triglyceride levels were higher at 3 and 6 months but lower at 12 months in *Clk^{Δ19/Δ19} Apoe^{−/−}* mice compared with controls (Figure 6A). Hepatic levels of TBARS, cholesterol (not shown), and free fatty acids increased with age in these mice (Figure 6A). Plasma ALT levels were significantly higher only in older mice, but β-HB levels were significantly reduced (Figure 6B). *Clk^{Δ19/Δ19} Apoe^{−/−}* livers assimilated more fatty acids from plasma than did control livers in mice of all ages (Figure 6C). More lipid accumulation as droplets was evident in 2- and 10-month-old *Clk^{Δ19/Δ19} Apoe^{−/−}* livers after Oil Red O staining (Figure 6D). H&E staining showed increased ballooning with age (Figure 6E). Electron microscopy showed accumulation of larger lipid droplets in 10-month-old *Clk^{Δ19/Δ19} Apoe^{−/−}* mice (Figure 6F). *Clk^{Δ19/Δ19} Apoe^{−/−}* livers showed more macrophage staining (Figure 6G) and had more TUNEL-positive cells (Figure 6H) than controls. Binding of HIF1α to the *Cd36* promoter was higher in *Clk^{Δ19/Δ19} Apoe^{−/−}* mice than in controls (Figure 6I). Livers of 12-month-old *Clk^{Δ19/Δ19} Apoe^{−/−}* mice were larger and showed micronodular cirrhosis (Figure 6J). These studies indicated that chow-fed *Clk^{Δ19/Δ19} Apoe^{−/−}* mice develop steatohepatitis and cirrhosis with age.

We then concentrated on understanding factors contributing to cirrhosis. Three-month-old *Clk^{Δ19/Δ19} Apoe^{−/−}* mice had higher plasma triglycerides, whereas 12-month-old mice had lower plasma triglyceride levels, than *Apoe^{−/−}* mice (Figure 7A). Triglyceride production studies in lipase-inhibited mice showed that *Clk^{Δ19/Δ19} Apoe^{−/−}* mice produced more triglyceride-containing lipoproteins at 3 months but produced less of these lipoproteins at 1 year compared with *Apoe^{−/−}* mice (Figure 7B). Activity and mRNA levels of *Mttp* were higher in young *Clk^{Δ19/Δ19} Apoe^{−/−}* animals but lower in older mice (Figure 7C). These studies showed that young *Clk^{Δ19/Δ19} Apoe^{−/−}* mice produce more hepatic lipoproteins, probably because of increased *Mttp* and *Dgat2* expression. With increasing age, lipoprotein production and *Mttp* expression decrease in these mice.

Younger *Clk^{Δ19/Δ19} Apoe^{−/−}* mice showed no difference in fatty acid β-oxidation compared with *Apoe^{−/−}* mice; however, 12-month-old *Clk^{Δ19/Δ19} Apoe^{−/−}* mice showed reduced β-oxidation as well as reduced expression of *Pparα*, *Pgc1α*, *Pgc1β*, and *Cpt1* (Figure 7D). Livers of older *Clk^{Δ19/Δ19} Apoe^{−/−}* mice assimilated significantly higher amounts of i.p.-injected OA (Figure 7E). Protein and mRNA levels of CD36 were significantly (approximately 5-fold) higher in older mice (Figure 7F). These studies show that livers of older *Clk^{Δ19/Δ19} Apoe^{−/−}* mice take up more fatty acids but produce fewer lipoproteins and store less triglyceride.

There were significant reductions of *Egln2*, *Egln1*, and *Egln3* mRNA levels but no effect on *Hif1α* and *Hif1β* mRNA levels (Figure 7G). Nonetheless, protein levels of HIF1α increased in *Clk^{Δ19/Δ19} Apoe^{−/−}* mice (Figure 7F). In the ER stress pathway, only *Ire1α* levels were significantly increased (Figure 7H). Further, there were modest changes in the proto-oncogenes and tumor suppressor genes, indicating a carcinogenic response. In contrast to these modest changes, we observed that mRNA levels of *Tnfα* and *Il6* increased 5- to 10-fold in older *Clk^{Δ19/Δ19} Apoe^{−/−}* mice compared with *Apoe^{−/−}* mice, indicating significant upregulation of the inflammatory response. In short, *Clk^{Δ19/Δ19} Apoe^{−/−}* mice showed reduced expression of genes in lipoprotein production and β-oxidation but increased expression of inflammatory response genes with age compared with *Apoe^{−/−}* mice. These changes may represent, or cause, a transition from NASH to cirrhosis.

LPS induces macronodular cirrhosis in Clk^{Δ19/Δ19} Apoe^{−/−} mice. *Clk^{Δ19/Δ19} Apoe^{−/−}*, but not *Apoe^{−/−}*, mice injected with LPS developed macronodular cirrhosis (Figure 8A). LPS-injected *Clk^{Δ19/Δ19} Apoe^{−/−}* mice had lower hepatic triglyceride (Figure 6B), higher TBARS (Figure 8B), higher plasma ALT levels, and lower β-HB (Figure 8C) than *Apoe^{−/−}* mice. *Clk^{Δ19/Δ19} Apoe^{−/−}* livers took up fewer fatty acids (Figure 8D) but more 3-3′-dioctadecylindocarbocyanine–labeled (DiI-labeled) acetylated LDL (AcLDL) (Figure 8E). They showed less β-oxidation (Figure 8F). Histologic analyses showed less lipid accumulation but more macrophages and some hyperplasia (Figure 8G). Gene expression analysis showed reduced expression of *Egln2*, *Egln1*, and *Egln3* and high expression of *Cd36* (Supplemental Figure 9A). Expression of genes involved in lipoprotein assembly and fatty acid oxidation decreased, whereas expression of those involved in lipogenesis increased (Supplemental Figure 9B). There were significant increases in inflammatory markers (Supplemental Figure 9C) and cancer markers (Supplemental Figure 9D) with modest effect on ER stress genes (Supplemental Figure 9E). These studies indicate that, compared with *Apoe^{−/−}* mice, *Clk^{Δ19/Δ19} Apoe^{−/−}* mice express higher amounts of genes involved in inflammation
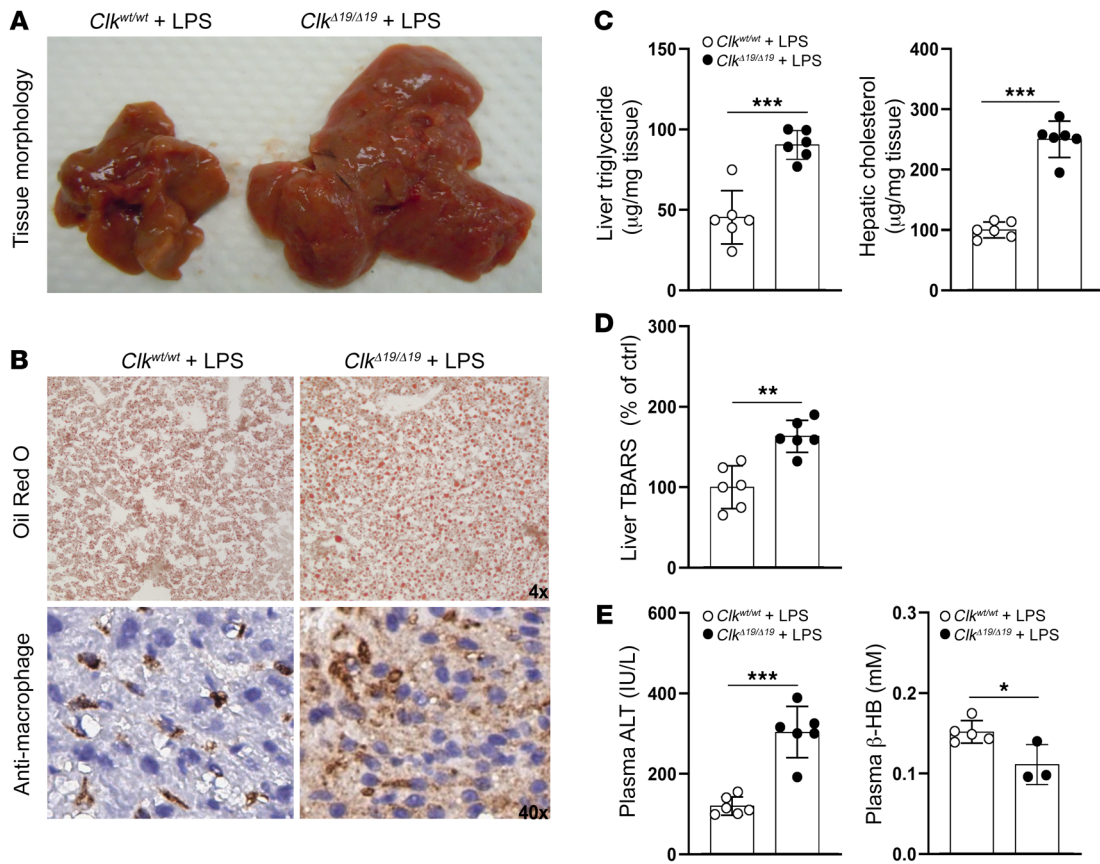
Figure 4. LPS-induced hepatosteatosis and cirrhosis in $Clk^{\Delta19/\Delta19}$ mice. Male (8-month-old) $Clk^{\Delta19/\Delta19}$ and $Clk^{wt/wt}$ mice on a chow diet were fed a Western diet for 2 months and injected i.p. with LPS (0.25 mg/kg per injection, 3 times on alternate days). Mice then continued on a Western diet for an additional 2 months, and livers and plasma were collected for analyses at the end (n = 6 per group). (**A**) Livers from LPS-injected $Clk^{\Delta19/\Delta19}$ mice showed hepatomegaly and micronodular cirrhosis. Pictures are representative of 2 experiments. (**B**) Frozen liver sections were stained with Oil Red O, H&E, and anti-macrophage antibodies. Representative of 2 experiments. (**C** and **D**) Liver pieces were used to measure triglyceride, cholesterol (**C**), and TBARS (**D**) levels. Mean ± SD; **$P < 0.01$, ***$P < 0.0001$, Welch's 2-tailed t test. (**E**) Plasma ALT and β-HB levels were measured in LPS-injected $Clk^{\Delta19/\Delta19}$ mice. Mean ± SD; *$P < 0.05$, ***$P < 0.0001$, Welch's 2-tailed t test.

and cancer when challenged with LPS, suggesting a transition from cirrhosis to carcinogenesis.

$CoCl_2$ induces HCC in $Clk^{\Delta19/\Delta19}$ Apoe$^{-/-}$ mice. To explore the effects of HIF1α activation in $Clk^{\Delta19/\Delta19}$ Apoe$^{-/-}$ mice, we injected mice with $CoCl_2$ and compared them with $CoCl_2$-injected Apoe$^{-/-}$ mice. Livers of $CoCl_2$-injected $Clk^{\Delta19/\Delta19}$ Apoe$^{-/-}$ mice had solid tumors (Figure 9A). $CoCl_2$ had no effect on hepatic *Hif1α* and *Hif1β* mRNA levels but significantly reduced levels of *Egln1* and *Egln3* mRNA (Figure 9B) and increased *Vegf* mRNA in $Clk^{\Delta19/\Delta19}$ Apoe$^{-/-}$ compared with Apoe$^{-/-}$ mice. In addition, *Cd36* mRNA levels increased significantly in $Clk^{\Delta19/\Delta19}$ Apoe$^{-/-}$ mice compared with Apoe$^{-/-}$ mice (Figure 9B). Western blotting showed significant increases in HIF1α and CD36, decreases in PHD proteins, but no change in HIF1β and β-actin protein levels (Figure 9C). Immunohistochemistry showed increased HIF1α and CD36 protein levels and macrophage staining (Figure 9D). Expression levels of ER response genes *Ire1α*, *Xbp1*, and *Bip* were higher (Figure 9E). In addition, there was significant induction of CCAAT/enhancer-binding protein homologous protein (CHOP). *Tnfα*, *Il6*, and *Tlr4* mRNA levels increased more than 10-fold, indicating a significant inflammatory response. Levels of the proto-oncogenes

Mdm2, *C-myc*, and *Bcl2* increased significantly, whereas the level of the tumor suppressor gene *Trp53* decreased significantly, which suggests carcinogenesis. Indeed, staining showed hyperplasia and no lipid deposition (Figure 9F). These studies suggest that $CoCl_2$ treatment increases expression of HIF1α in $Clk^{\Delta19/\Delta19}$ Apoe$^{-/-}$ mice compared with Apoe$^{-/-}$ mice and induces an inflammatory response and expression of genes that favor carcinogenesis. Thus, pathologic upregulation of these genetic programs may be involved in the development of HCCs.

$CoCl_2$ induces HIF1α in macrophages. We were surprised by the reduced lipid accumulation after Oil Red O staining in $CoCl_2$-injected $Clk^{\Delta19/\Delta19}$ mice compared with controls (Figure 9F). Consistent with reduced Oil Red O staining, triglyceride content was lower in $Clk^{\Delta19/\Delta19}$ Apoe$^{-/-}$ mice (Figure 10A); however, liver TBARS (Figure 10B) and plasma ALT (Figure 10C) levels were significantly higher. In contrast, plasma β-HB levels were reduced (Figure 10C). To explore reasons for the reduced hepatic triglyceride levels, we studied fatty acid uptake. Despite significant increases in *Cd36* mRNA and protein levels (Figure 9, B and C), the livers (Figure 10D) and isolated hepatocytes (Figure 10E) from $Clk^{\Delta19/\Delta19}$ Apoe$^{-/-}$ mice took up fewer fatty acids. To explain this discrepancy, we explored
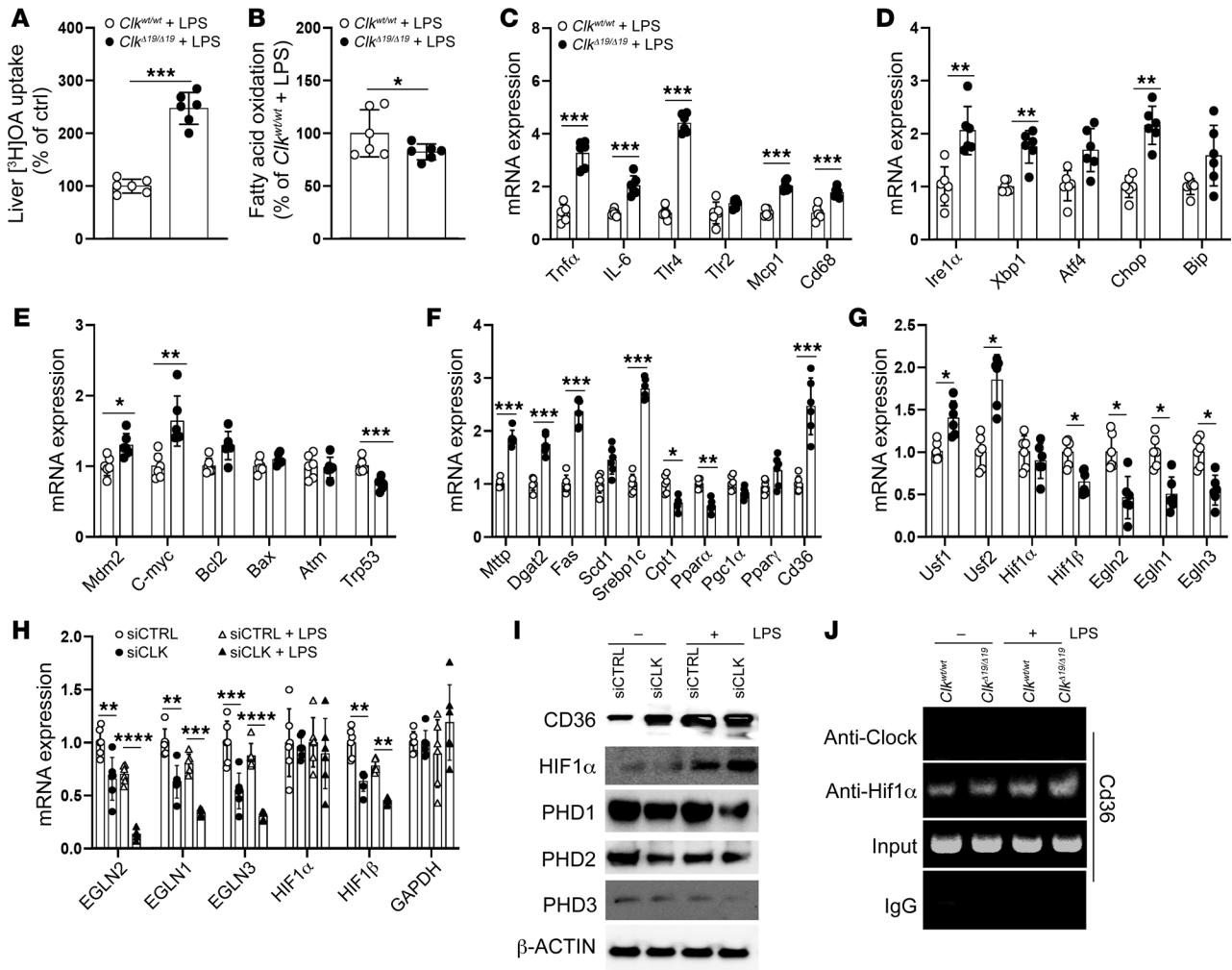
Figure 5. LPS induces HIF1α and CD36 in *Clk^Δ19/Δ19* mice. Mice were treated with LPS as described in Figure 4 and used to study fatty acid uptake and oxidation (*n* = 6 per group). (**A**) Hepatic fatty acid uptake. LPS-injected *Clk^Δ19/Δ19* mice took up more [³H]OA. Mean ± SD; ***P < 0.001, Welch's 2-tailed *t* test. (**B**) Fatty acid oxidation. Fresh liver slices from LPS-injected *Clk^Δ19/Δ19* mice were incubated with [¹⁴C]PA (0.2 μCi) for 2 hours, and radiolabeled CO₂ trapped on filter papers soaked with phenylethylamine was quantified. Mean ± SD; *P < 0.05, Welch's 2-tailed *t* test. (**C–G**) Quantification of different indicated mRNAs in livers of LPS-injected *Clk^Δ19/Δ19* and *Clk^wt/wt* mice. Mean ± SD; *P < 0.05, **P < 0.01, ***P < 0.001, multiple *t* tests. (**H** and **I**) Human hepatoma Huh7 cells were transfected with *siCTRL* or *siCLK*. After 48 hours, they were treated or not with LPS (25 ng/mL) for 12 hours. RNA was isolated to quantify mRNA levels of indicated genes (**H**) (mean ± SD; **P < 0.01, ***P < 0.001, ****P < 0.0001, multiple *t* tests; data representative of 2 experiments) and protein levels (**I**). (**J**) Livers from *Clk^Δ19/Δ19* and *Clk^wt/wt* mice injected or not with LPS were used to study the binding of CLOCK and HIF1α by ChIP assay. Data are representative of 2 experiments.

several possibilities. First, we considered increased β-oxidation. However, we found reduced β-oxidation (Figure 10E) and lower expression of genes (*Pparα* and *Cpt1*) in this pathway (Figure 10F). Second, we considered the possibility that *Clk^Δ19/Δ19 Apoe^−/−* mice produce more lipoproteins. However, we observed lower expression of genes involved in lipoprotein assembly and secretion (*Mttp*, *Dgat2*, and *Scd1*; Figure 10F). These studies showed that lipoprotein production were diminished. Therefore, reduced oxidation and lipoprotein production cannot explain lower hepatosteatosis.

Abnormally high mRNA levels of inflammatory response genes (Figure 9E) suggested a role for macrophages. Therefore, we hypothesized that CoCl₂ may induce CD36 in hepatic Kupffer cells in *Clk^Δ19/Δ19 Apoe^−/−* mice. Indeed, isolated Kupffer cells took up more oxidized LDL (oxLDL; Figure 10G). Further, we studied the effect of oxLDL and CoCl₂ on *Hif1α* and *Cd36* expression in a J774

mouse macrophage cell line treated with *siClk* or *siHifF1α* (Supplemental Figure 10). *siClk* and *siHif1α* significantly increased *Cd36* but had no effect on β-actin mRNA and protein (Supplemental Figure 10, A–C) compared with *siCtrl*. OxLDL and CoCl₂ further increased *Cd36* mRNA and protein levels in *siClk*-treated cells (Supplemental Figure 10, A and C). OxLDL and CoCl₂ increased HIF1α protein levels, but not mRNA levels, in *siClk*-treated cells. Increases in HIF1α protein levels were not seen in *siHif1α*-treated cells (Supplemental Figure 10C). We also studied induction of HIF1α and CD36 proteins in control and CLOCK-knockdown cells subjected to serum shock and exposed to oxLDL for various times (Supplemental Figure 10D). HIF1α and CD36 proteins levels increased within 4 hours, and this response was transient in *shCtrl*-treated cells, indicating temporal regulation. In *shClk*-treated cells, CD36 levels were induced faster, reached much higher lev-
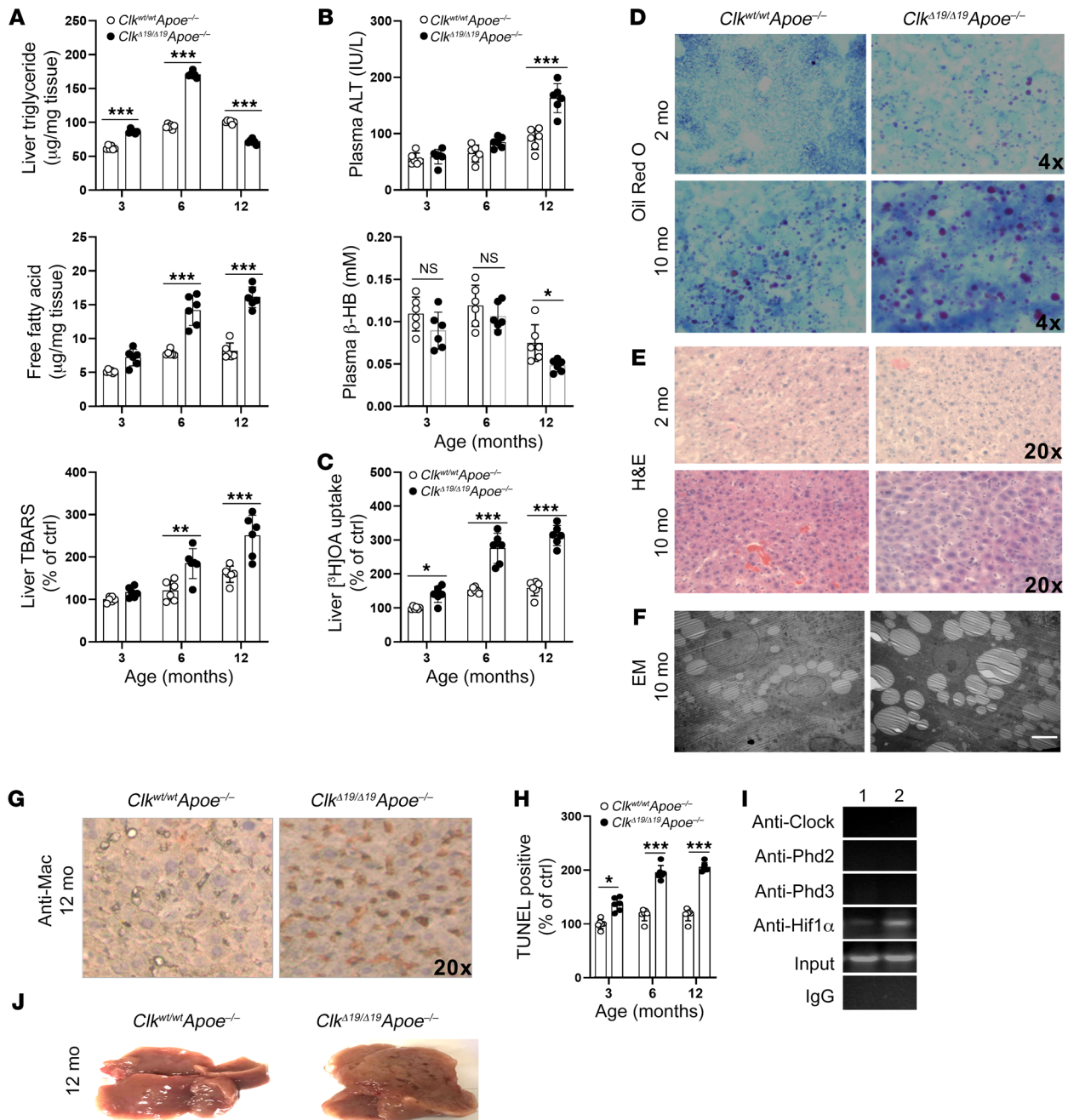
Figure 6. Age-dependent changes in hepatic lipid metabolism in *Clk^Δ19/Δ19^ Apoe^-/-^* mice. Male *Clk^Δ19/Δ19^ Apoe^-/-^* and *Apoe^-/-^* (*Clk^wt/wt^ Apoe^-/-^*) mice were fed a chow diet, and livers and plasma were collected at 3 months (2–3 months, *n* = 8 per group), 6 months (5–6 months, *n* = 6 per group), or 12 months (10–12 months, *n* = 12 per group). Mean ± SD; *$P < 0.05$, **$P < 0.01$, ***$P < 0.001$, multiple *t* tests. (**A**) Hepatic triglyceride, free fatty acid, and TBARS levels measured using kits. (**B**) Plasma ALT levels were high in older *Clk^Δ19/Δ19^ Apoe^-/-^* mice. In contrast, plasma β-HB concentrations were low in older *Clk^Δ19/Δ19^ Apoe^-/-^* mice. (**C**) [^{3}H]OA was injected i.p. into mice. Hepatic radioactivity was measured after 2 hours. (**D** and **E**) Liver sections were stained with Oil Red O (**D**) and H&E (**E**) staining. Data are representative of 2 independent experiments. (**F**) Electron microscopy (scale bar: 100 μm) showed more lipid droplets in older *Clk^Δ19/Δ19^ Apoe^-/-^* mice. Data are representative of 2 experiments. (**G**) Macrophage infiltration was determined by staining for CD68 in 12-month-old mice. Data are representative of 2 experiments. (**H**) Liver apoptotic cells were detected by TUNEL staining and were quantified. (**I**) Livers from mice (12 months old, chow diet) were used to study the binding of different proteins to the HIF1α binding site in the *Cd36* promoter. Data are representative of 2 experiments. (**J**) Representative photograph of livers in 12-month-old mice.

els, and remained high for longer times. Thus, CLOCK-deficient J774 cells respond to oxLDL and CoCl$_2$ by augmenting HIF1α and CD36 protein levels. Consistent with these studies, Kupffer cells isolated from *Clk^Δ19/Δ19^ Apoe^-/-^* mice and treated with CoCl$_2$ took up

more DiI-AcLDL (Figure 10H) and expressed more *Cd36* mRNA (Figure 10I). Further, the yield of Kupffer cells from CoCl$_2$-treated *Clk^Δ19/Δ19^ Apoe^-/-^* mice was 3-fold higher than that from CoCl$_2$-treated *Apoe^-/-^* mice. HIF1α binding to the *Cd36* promoter increased
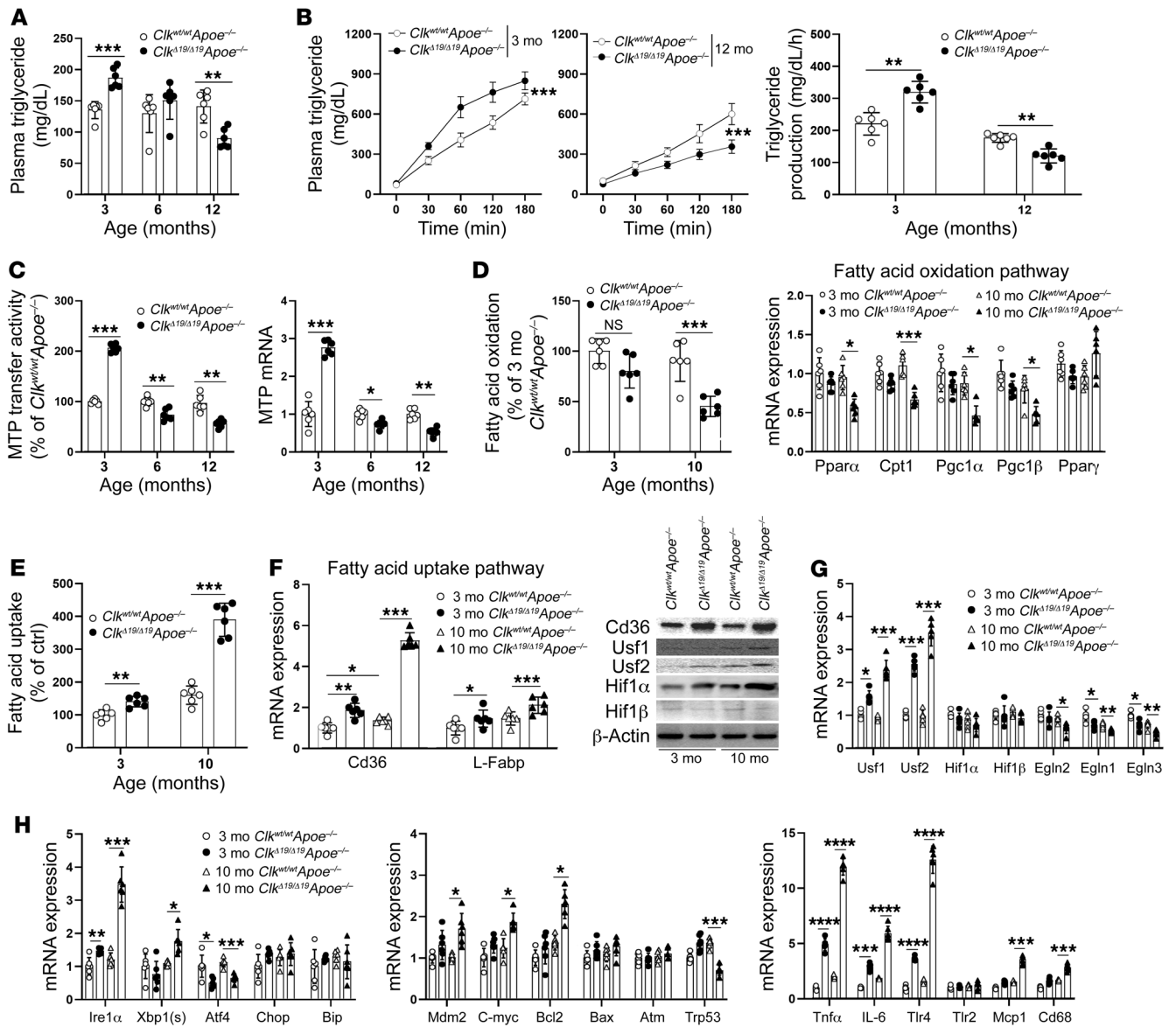
Figure 7. Factors contributing to cirrhosis in *Clk^{Δ19/Δ19} Apoe^{-/-}* mice. Male mice (*n* = 6 per group) were fed a chow diet ad libitum, and livers and plasma were analyzed at indicated ages. (**A**) Plasma triglyceride levels were higher in younger mice but were lower in older *Clk^{Δ19/Δ19} Apoe^{-/-}* mice. (**B**) Overnight-fasted animals were injected with poloxamer 407 to inhibit lipases, and plasma triglyceride levels were determined at indicated times. Triglyceride production was higher in younger mice but was lower in older *Clk^{Δ19/Δ19} Apoe^{-/-}* mice. (**C**) Hepatic MTP activity (left) and mRNA levels (right) decreased with age in chow-fed male *Clk^{Δ19/Δ19} Apoe^{-/-}* mice. Similar changes in hepatic MTP protein levels were detected by Western blotting (data not shown). (**D**) Liver pieces in triplicate were incubated with [^{14}C]PA for 2 hours to measure fatty acid oxidation. Fatty acid oxidation (left) and expression of genes in fatty acid oxidation (right) were reduced in 12-month-old chow-fed male *Clk^{Δ19/Δ19} Apoe^{-/-}* mice. (**E**) Hepatic fatty acid uptake increased in older *Clk^{Δ19/Δ19} Apoe^{-/-}* mice. (**F**) mRNA levels of genes in fatty acid uptake (*Cd36* and *L-Fabp*) were quantified by quantitative real-time PCR (left). Indicated proteins were identified by Western blotting using specific antibodies (right). Data are representative of 2 experiments. (**G**) *Egln* mRNA levels were reduced in older *Clk^{Δ19/Δ19} Apoe^{-/-}* mice. (**H**) Quantification of selected mRNAs in inflammatory response, ER stress, and carcinogenesis in livers of 12-month-old chow-fed male mice. Mean ± SD; *$P < 0.05$, **$P < 0.01$, ***$P < 0.001$, ****$P < 0.0001$, 2-way ANOVA, Šidák's multiple-comparisons test.

significantly in Kupffer cells isolated from *Clk^{Δ19/Δ19}* and *Clk^{Δ19/Δ19} Apoe^{-/-}* mice (Figure 10J). These studies suggest that CD36 is regulated similarly in hepatocytes and Kupffer cells in mice that express the CLOCK mutant protein. Thus, it is likely that, in the early stages of liver disease, CD36 expression increases in hepatocytes, leading to increased fatty acid uptake and steatosis. In advanced liver diseases, macrophages that express higher amounts of CD36 take up more modified lipoproteins.

Different pathways and molecules in the development of NAFLD in Clk^{Δ19/Δ19} mice. Data from previous figures are summarized in Supplemental Figures 11 and 12 in an attempt to portray a comprehensive overview of various changes observed in *Clk^{Δ19/Δ19}* and *Clk^{Δ19/Δ19} Apoe^{-/-}* mice with age and after various environmental insults. Young *Clk^{Δ19/Δ19}* mice did not show steatosis (Supplemental Figure 11A). However, older mice developed steatosis on a chow diet, and this was accelerated when mice were fed a Western diet.
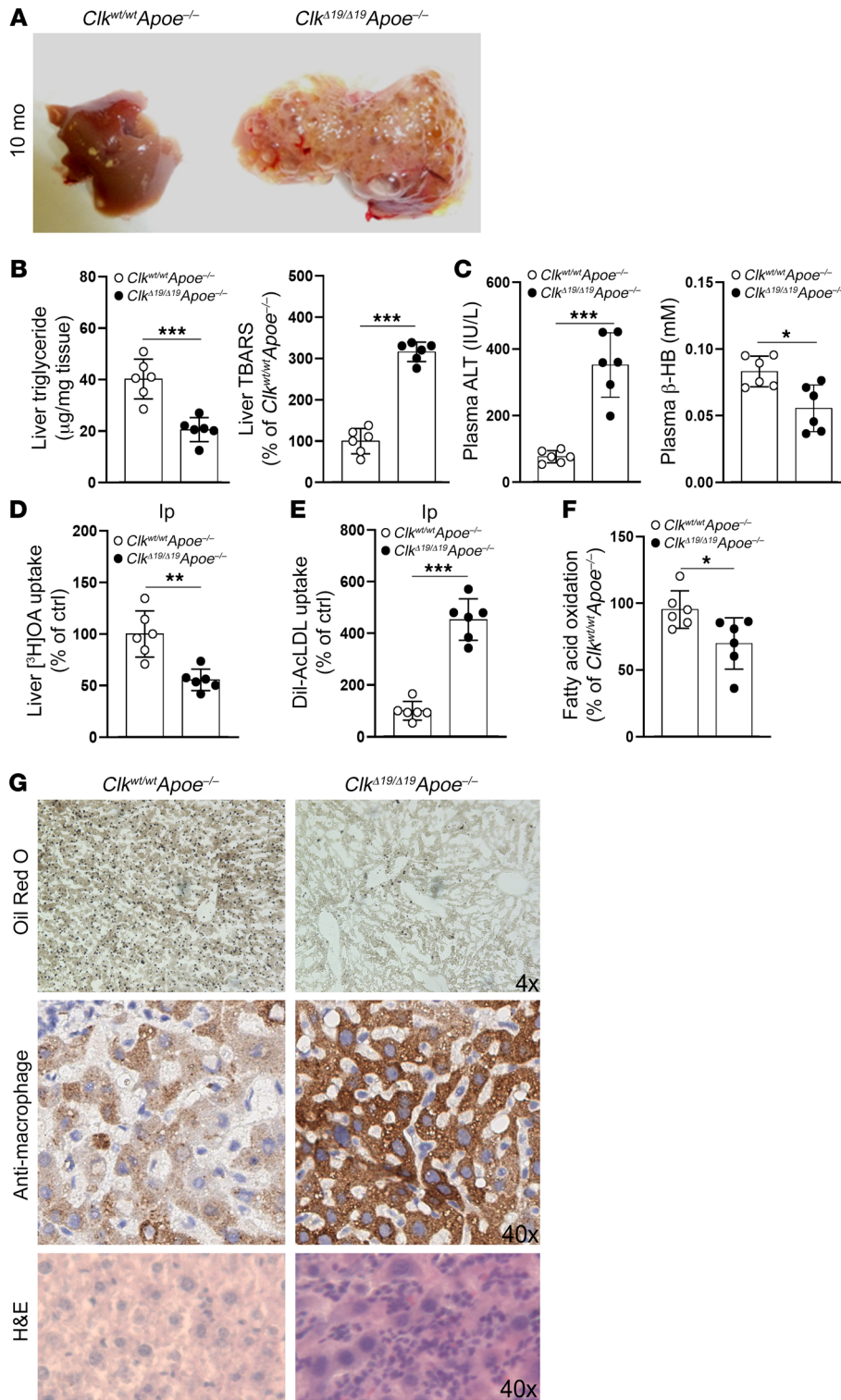
Figure 8. LPS induces cirrhosis and carcinoma in *Clk^{Δ19/Δ19} Apoe^{-/-}* mice. Male (10-month-old) *Clk^{Δ19/Δ19} Apoe^{-/-}* and *Apoe^{-/-}* mice fed a chow diet were injected i.p. with LPS (0.25 mg/kg) 3 times on alternate days. Two months after the last injection, plasma and liver were collected (*n* = 6 per group). Other animals were used for [³H]OA or carbon-14–labeled OA ([¹⁴C]OA) uptake and oxidation (*n* = 6 per group), respectively, or for DiI-labeled AcLDL uptake (*n* = 6 per group). (**A**) Livers from LPS-injected *Clk^{Δ19/Δ19} Apoe^{-/-}* mice showed macronodular cirrhosis. (**B**) Liver triglyceride decreased but liver TBARS levels increased in LPS-injected *Clk^{Δ19/Δ19} Apoe^{-/-}* mice. Mean ± SD; ****P* < 0.001, unpaired Welch's 2-tailed *t* test. (**C**) Plasma ALT levels were higher in LPS-injected *Clk^{Δ19/Δ19} Apoe^{-/-}* mice. In contrast, plasma β-HB concentrations were lower in LPS-injected *Clk^{Δ19/Δ19} Apoe^{-/-}* mice. Mean ± SD; **P* < 0.05, ****P* < 0.001, unpaired Welch's 2-tailed *t* test. (**D**) Hepatic uptake of [³H]OA was lower in LPS-injected *Clk^{Δ19/Δ19} Apoe^{-/-}* mice. Mean ± SD; ***P* < 0.01, unpaired Welch's 2-tailed *t* test. (**E**) DiI-labeled AcLDL uptake was high after 2 hours in livers of *Clk^{Δ19/Δ19} Apoe^{-/-}* mice injected with DiI-labeled AcLDL (5 μg/mL). Mean ± SD; ****P* < 0.001, unpaired Welch's 2-tailed *t* test. (**F**) Fatty acid oxidation was decreased in LPS-injected *Clk^{Δ19/Δ19} Apoe^{-/-}* mice. Mean ± SD; **P* < 0.001, unpaired Welch's 2-tailed *t* test. (**G**) Livers were stained with Oil Red O (top), anti-macrophage antibodies (middle), and H&E (bottom). Data are representative of 2 experiments.

Exposure to LPS or CoCl₂ induced cirrhosis. Thus, CLOCK deficiency increases the risk for steatosis, steatohepatitis, and cirrhosis. Although young *Apoe^{-/-}* mice do not exhibit steatosis, young *Clk^{Δ19/Δ19} Apoe^{-/-}* mice exhibit both steatosis and NASH, and these mice develop cirrhosis with age on a chow diet. Thus, apoE deficiency is an additional risk factor for steatohepatitis and cirrhosis in *Clk^{Δ19/Δ19}* mice. It remains undetermined whether increased plasma lipoproteins and/or apoE deficiency are primary contrib-

uting factors to cirrhosis. *Clk^{Δ19/Δ19} Apoe^{-/-}* mice injected with LPS or CoCl₂ developed cirrhosis and HCC.

Hepatic triglycerides increased in *Clk^{Δ19/Δ19}* mice with age and Western diet (Supplemental Figure 11B). LPS and CoCl₂ injections reduced hepatic triglyceride in these mice. The *Clk^{Δ19/Δ19} Apoe^{-/-}* livers had lower triglyceride, and these levels decreased further after LPS and CoCl₂ injections. Hepatic fatty acid uptake increased with age and Western diet in both *Clk^{Δ19/Δ19}* and *Clk^{Δ19/Δ19} Apoe^{-/-}*
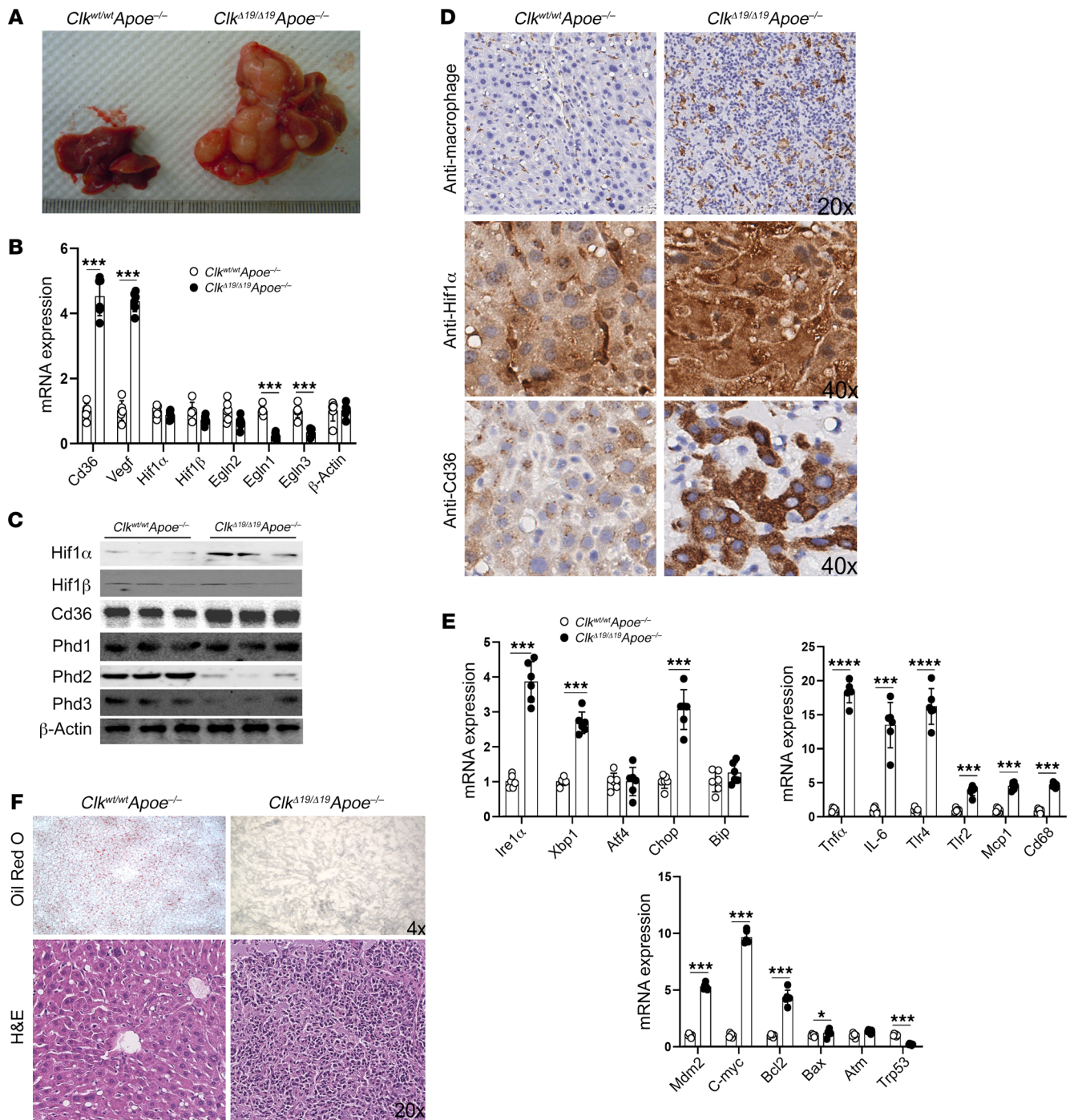
Figure 9. CoCl$_2$ induces HCC in *Clk*$^{\Delta 19/\Delta 19}$ *Apoe*$^{-/-}$ mice. Male *Clk*$^{\Delta 19/\Delta 19}$ *Apoe*$^{-/-}$ and *Apoe*$^{-/-}$ (10-month-old, ad libitum chow-fed) mice were injected i.p. 3 times on alternate days with CoCl$_2$ (30 mg/kg) and continued on the same diet for an additional 2 months. (**A**) *Clk*$^{\Delta 19/\Delta 19}$ *Apoe*$^{-/-}$ mice injected with CoCl$_2$ developed HCC. (**B**) Expression of genes in hypoxia and *Cd36*. Mean ± SD; ***$P < 0.001$, multiple t tests. (**C**) HIF1α and CD36 protein levels increased in livers of CoCl$_2$-injected *Clk*$^{\Delta 19/\Delta 19}$ *Apoe*$^{-/-}$ mice. (**D**) HIF1α and CD36 protein levels and macrophages increased in livers of CoCl$_2$-injected *Clk*$^{\Delta 19/\Delta 19}$ *Apoe*$^{-/-}$ mice. Data are representative of 2 experiments. (**E**) mRNA levels of selected genes in ER stress, inflammatory response, and carcinogenesis. Mean ± SD; *$P < 0.05$, ***$P < 0.001$, ****$P < 0.0001$, multiple t tests. (**F**) Livers were stained with Oil Red O stains (top) and H&E stains (bottom). Livers of CoCl$_2$-injected *Clk*$^{\Delta 19/\Delta 19}$ *Apoe*$^{-/-}$ mice showed less lipid staining and more hyperplasia. Data are representative of 2 experiments.

mice (Supplemental Figure 11C). Hepatic TBARS increased in both *Clk*$^{\Delta 19/\Delta 19}$ and *Clk*$^{\Delta 19/\Delta 19}$ *Apoe*$^{-/-}$ mice in early stages of disease, reached maximum levels in cirrhotic livers, and remained high in HCC (Supplemental Figure 11D). It is likely that high hepatic

TBARS is a good indicator of a cirrhotic liver in mice. Plasma ALT levels increased in both animal models with age, Western diet, and LPS/CoCl$_2$ treatments (Supplemental Figure 11E); therefore, ALT could be a good marker for severity of the disease.
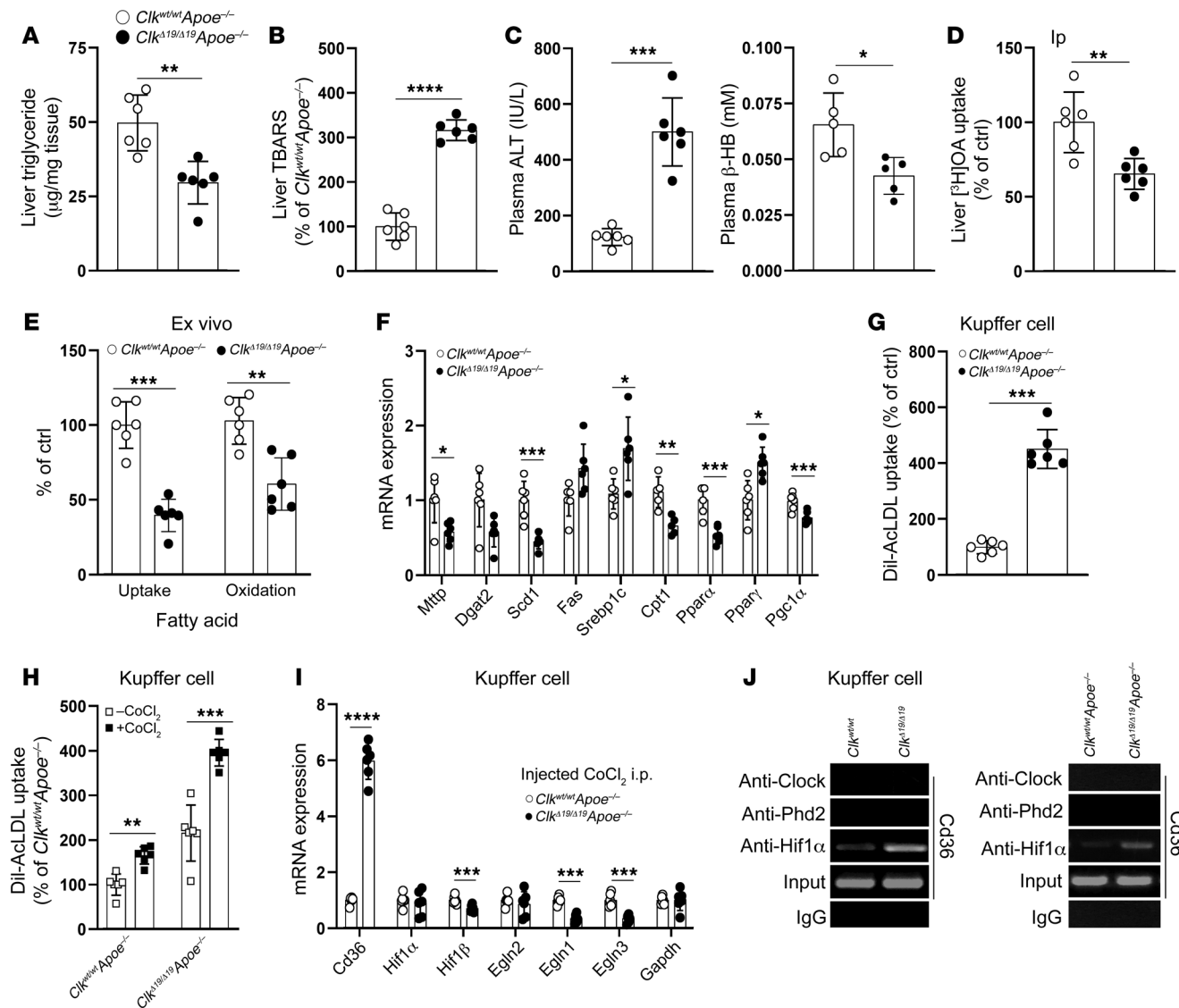
Figure 10. CoCl₂ induces HIF1α in macrophages in *Clk^Δ19/Δ19* Apoe^−/− mice. Animals were treated with CoCl₂ as described in Figure 9 and used to collect tissues (*n* = 6 per group), to study hepatic [³H]OA uptake or [¹⁴C]OA oxidation (*n* = 6 per group), or for isolation of Kupffer cells (*n* = 6 per group). (**A** and **B**) Triglyceride levels decreased (**A**) but TBARS increased (**B**) in livers of CoCl₂-injected *Clk^Δ19/Δ19* Apoe^−/− mice. (**C**) Plasma ALT levels increased in CoCl₂-injected *Clk^Δ19/Δ19* Apoe^−/− mice. In contrast, plasma β-HB concentrations decreased in CoCl₂-injected *Clk^Δ19/Δ19* Apoe^−/− mice. (**D**) Livers from CoCl₂-injected *Clk^Δ19/Δ19* Apoe^−/− mice assimilated less [³H]OA than controls. (**E**) Liver slices from CoCl₂-injected *Clk^Δ19/Δ19* Apoe^−/− mice were used to study fatty acid uptake and oxidation. (**F**) Expression of lipoprotein assembly and β-oxidation genes was reduced in CoCl₂-injected *Clk^Δ19/Δ19* Apoe^−/− mice. Mean ± SD; *P < 0.05, **P < 0.01, ***P < 0.001, ****P < 0.0001, multiple *t* tests. (**G**) Kupffer cells isolated from CoCl₂-injected *Clk^Δ19/Δ19* Apoe^−/− mice took up more Dil-labeled AcLDL (5 μg/mL). Kupffer cells were incubated with Dil-labeled AcLDL (5 μg/mL) for 4 hours. Cells were washed, lipids were extracted, and dye was measured at 485 nm. (**H**) Kupffer cells isolated from CoCl₂-injected *Clk^wt/wt* Apoe^−/− and *Clk^Δ19/Δ19* Apoe^−/− mice were incubated with Dil-AcLDL. Mean ± SD; ***P < 0.001, 2-way ANOVA, Šidák's multiple-comparisons test. (**I**) mRNA levels of different genes in isolated Kupffer cells from CoCl₂-injected mice. Mean ± SD; ***P < 0.001, ****P < 0.0001, multiple *t* tests. (**J**) ChIP assays were performed in Kupffer cells isolated from livers of indicated mice to study the binding of HIF1α to the *Cd36* promoter. Data are representative of 2 experiments.

Clk^Δ19/Δ19 mice showed reduced expression of *Cpt1* (Supplemental Figure 11F). It is likely that low *Cpt1* mRNA levels in *Clk^Δ19/Δ19* mice may be an early indicator of impaired fatty acid β-oxidation that could contribute to steatosis. We observed that *Fas* and *Mttp* mRNA increased in *Clk^Δ19/Δ19* mice with age and a Western diet and remained high after other interventions. Surprisingly, older *Clk^Δ19/Δ19* Apoe^−/− mice injected with LPS or CoCl₂ had reduced *Fas* and *Mttp* expression. Thus, in advanced diseases, hepatic lipid synthesis and lipoprotein assembly might be downregulated.

In general, *Cd36* mRNA levels increase with age, Western diet, and CoCl₂ injection in *Clk^Δ19/Δ19* mice (Supplemental Figure 11F). Our studies suggest that, in early stages, CD36 increases in hepatocytes and is associated with increased fatty acid uptake. In advanced diseases, CD36 increases in macrophages and may be associated with increased uptake of modified lipoproteins.

Both *Clk^Δ19/Δ19* and *Clk^Δ19/Δ19* Apoe^−/− mice showed increases only in mRNA levels of *Ire1α* and its downstream target *Xbp1* (Supplemental Figure 12). Also, diets and other interventions failed to

induce other arms of the ER stress pathway. Increases in Ire1α pathway may contribute to increases in plasma ALT. We have shown that the Ire1α pathway may increase expression of transaminases via the JNK pathway (29). These studies suggest that CLOCK mutant protein selectively upregulates the Ire1α pathway.

$Clk^{Δ19/Δ19}$ mice fed different diets and challenged with LPS or $CoCl_2$ showed modest increases (Supplemental Figure 11G) in *Tlr4* and *Il6* mRNA. However, $Clk^{Δ19/Δ19}$ $Apoe^{-/-}$ mice challenged with LPS or $CoCl_2$ showed greater increases (>10-fold) compared with controls (Supplemental Figure 11G). Genes involved in carcinogenesis did not differ between control and $Clk^{Δ19/Δ19}$ mice (Supplemental Figure 11H), but they were modestly increased or decreased in older $Clk^{Δ19/Δ19}$ $Apoe^{-/-}$ mice. However, LPS (approximately 5-fold change) and $CoCl_2$ (approximately 5- to 10-fold change) significantly increased *C-myc* and *Bcl2* genes but decreased *Trp53* in $Clk^{Δ19/Δ19}$ $Apoe^{-/-}$ mice. Thus, changes in the expression of inflammation and cancer genes are associated with advanced liver diseases, such as cirrhosis and HCC, in $Clk^{Δ19/Δ19}$ $Apoe^{-/-}$ mice.

In these studies, we did not see any change in HIF1α mRNA levels. However, a constant feature of all $Clk^{Δ19/Δ19}$ and $Clk^{Δ19/Δ19}$ $Apoe^{-/-}$ mice was age-dependent reduction in *Egln* mRNA levels (Supplemental Figure 11I). Therefore, reduction in *Phd* mRNA levels and associated increases in HIF1α protein levels could be significant contributing factors for age-dependent liver disease progression in $Clk^{Δ19/Δ19}$ mice.

Discussion

Here, we report that $Clk^{Δ19/Δ19}$ mice on WT and $Apoe^{-/-}$ backgrounds exhibit different stages of NAFLD. The progression of liver diseases is accelerated when $Clk^{Δ19/Δ19}$ mice are fed a high-cholesterol diet or in the presence of apoE deficiency. Injection of LPS to cholesterol-fed $Clk^{Δ19/Δ19}$ mice enhanced the inflammatory response and steatohepatitis; the same injection to $Clk^{Δ19/Δ19}$ $Apoe^{-/-}$ mice induced cirrhosis. Injection of $CoCl_2$ in $Clk^{Δ19/Δ19}$ and $Clk^{Δ19/Δ19}$ $Apoe^{-/-}$ mice induced cirrhosis and HCC, respectively. Molecular studies revealed that hepatic CD36 increased in these mice. Mechanistic studies identified HIF1α as a major regulator of CD36 and a key transcription factor that contributes to disease progression. Knockdown of HIF1α attenuated disease progression in $Clk^{Δ19/Δ19}$ mice. We showed that CLOCK regulates HIF1α protein levels by binding to the E-boxes in the promoters and modulating the expression of PHD proteins that regulate HIF1α protein stability. In CLOCK deficiency, PHD levels are low, and HIF1α levels are high. Under these conditions, HIF1α binds to the *Cd36* promoter to increase expression of CD36 and uptake of fatty acids by the liver. Thus, a regulatory mechanism involving circadian CLOCK, hypoxia signaling, and lipid metabolism protects against NAFLD.

Age-dependent studies in chow-fed $Clk^{Δ19/Δ19}$ mice provided some clues about the development of steatosis and steatohepatitis. Adolescent mice (<3 months old) did not accumulate significant amounts of hepatic triglyceride. However, these mice showed increased expression of genes in lipid synthesis and reduced expression of genes in β-oxidation. A combination of these changes should have caused steatosis. However, these mice also had increased expression of genes in lipoprotein assembly and secretion; we have shown previously that these mice produce more lipoproteins and display hypertriglyceridemia (15, 16, 30,

31). Based on our current and previous studies, we suggest that CLOCK deficiency affects several pathways. It upregulates lipid synthesis and inhibits β-oxidation. It also favors lipoprotein production to avoid steatosis and results in hypertriglyceridemia in young mice. However, in older mice, this balance is shifted toward more hepatic lipid accumulation.

Young $Clk^{Δ19/Δ19}$ $Apoe^{-/-}$ mice develop hepatosteatosis; however, older mice challenged with LPS or $CoCl_2$ have lower hepatic triglyceride levels and develop cirrhosis and HCC. Thus, hepatic disease starts with increased lipid uptake and accumulation and culminates with increased inflammatory and carcinogenic responses.

These studies identified 3 pathways — circadian rhythms, lipid uptake, and hypoxia — and 4 proteins — CLOCK, apoE, CD36, and HIF1α — that play roles in the pathogenesis of NAFLD. First, CLOCK is an important regulator of lipid uptake and hypoxia response under normoxic conditions by modulating the expression of PHD proteins. Second, apoE deficiency, along with CLOCK deficiency, contributes to liver disease. Third, CD36 plays a role in the uptake of fatty acids and the development of steatosis. Fourth, HIF1α regulates CD36 expression. Thus, circadian control mechanisms regulate lipid metabolism via hypoxia signaling.

Normally, HIF1α protein levels are low and increase under hypoxic conditions. HIF1α plays a role in fibrosis and in cancer progression (9, 32, 33) because of the presence of hypoxic conditions in fibrotic and cancerous liver tissues. Our studies point to involvement of HIF1α in the early stages of liver disease, such as steatosis and NASH, before the onset of hypoxic conditions. We propose that, under normoxic conditions, HIF1α is regulated by circadian rhythms, and increased expression of HIF1α might be a contributing factor for the pathogenesis of liver diseases when circadian rhythms are disrupted.

We identified HIF1α as a regulator of lipid uptake. In addition, we observed that increases in HIF1α were associated with reduced fatty acid oxidation. This is consistent with studies that showed that HIF1α and HIF2α reduced fatty acid oxidation under hypoxic conditions (34).

Our study was not designed to address the role of different liver cells in disease progression. We think all liver cells play an integral role in the development of NAFLD. We provide evidence for the involvement of hepatocytes and Kupffer cells using isolated cells. Both these cells express HIF1α and CD36 (34). In addition, hepatic endothelial cells also most likely play a role in disease progression.

The relevance of mouse models to human diseases is highly debated. Nevertheless, mouse models provide some understanding about molecules and pathways that could play roles in disease progression (35, 36). Here, we provide mouse models that show different stages of NAFLD. The observations made here in $Clk^{Δ19/Δ19}$ mice might be specific to these mice because of the expression of the dominant-negative CLOCK mutant protein. Conversely, these observations could be indirectly related to changes in circadian rhythms. Additional mouse models with disruptions in other circadian genes are needed to parse whether CLOCK deficiency and/or disruptions in circadian rhythms increase the risk for NAFLD.

It remains to be determined whether biochemical and molecular mechanisms described in these mouse models are also altered in other mouse models of NAFLD and in humans. If similar mechanisms are found in humans, these mouse models could

identify molecules that play critical roles in transition from one disease stage to another and different drugs that can prevent and reverse these diseases.

In summary, we demonstrate that normal CLOCK functions to protect against NAFLD. BMAL1 has been shown to protect against alcoholic liver disease (37). Thus, circadian genes, in general, may protect against both alcoholic and nonalcoholic liver diseases. In the absence of the normal CLOCK regulatory function, livers accumulate lipids and a cascade of events occurs, resulting in steatohepatitis and cirrhosis with age. The development of these pathologies is augmented by additional insults, such as apoE deficiency, LPS, and CoCl₂. Thus, deregulation of the CLOCK function might predispose mice to NAFLD. Different mouse models described here may be useful to explore additional molecular, biochemical, and physiologic pathways and to discover drugs that prevent liver diseases.

Methods

Fresh stock solutions of 0.4 M $CoCl_2$ or 0.25 M DMOG (Supplemental Table 1) were prepared in 0.9% NaCl, filtered, and added to the medium to obtain desired final concentrations. For i.p. injections, stock was prepared in sterile PBS. LPS was dissolved in PBS to obtain a concentration of 1 mg/mL. [9,10-³H(N)]Oleic acid ([³H]OA; 1 μCi/mL, 37 MBq, catalog NET289001MC), carbon-14–labeled OA (2.183 GBq/mmol, catalog PEC317150UC), and carbon-14–labeled palmitic acid (PA; 1 μCi/mL, 1.85 MBq, catalog NEC534050UC) were obtained from PerkinElmer. Adenoviruses expressing shRNA against mouse HIF1α (1 × 10¹¹ PFU/mL) were from Vector Biolabs.

Animals. C57BL/6J $Clk^{wt/wt}$, $Clk^{\Delta19/\Delta19}$, and $Apoe^{-/-}$ mice were from The Jackson Laboratory. $Clk^{\Delta19/wt}$ mice were bred to obtain $Clk^{wt/wt}$ and $Clk^{\Delta19/\Delta19}$ mice for experiments. $Clk^{\Delta19/\Delta19}$ and $Apoe^{-/-}$ mice were interbred to obtain male and female $Clk^{\Delta19/wt} Apoe^{-/-}$ mice. These mice were bred to obtain $Apoe^{-/-}$ and $Clk^{\Delta19/\Delta19} Apoe^{-/-}$ siblings for experiments (15). All mice were fed a chow diet (Supplemental Table 2) unless stated otherwise. To study the effects of different diets, age- and sex-matched littermates were placed on either a cholate-containing high-fat diet (Harlan Teklad, TD88051) or a high-cholesterol Western diet (Supplemental Table 2). In some experiments, mice were injected via tail vein with a single dose of lentiviruses expressing shRNA HIF1α (1 × 10⁹ PFU) or control viruses harboring no transgene (shRNA control). CoCl₂ and LPS were injected i.p. on alternate days, as described in the figure legends.

Plasma and tissue lipid analysis. Blood samples were obtained from the tail vein after a 4-hour fast. Total plasma triglycerides, cholesterol, β-HB, and free fatty acids were assayed using commercial kits (16, 17, 38). Plasma ALT and AST levels were measured using kits from Wako Pure Chemical Industries (38). Hepatic lipid peroxidation was assessed by measurement of TBARS (15–17, 38). Liver tissues (30–50 mg) were homogenized in buffer K, as previously described (16, 30). Lipids were extracted with chloroform/methanol and quantified using commercial kits (16).

Mouse hepatocytes and Kupffer cells. We isolated primary hepatocytes or Kupffer cells from different mice by collagenase perfusion, as previously described (17, 39, 40). To obtain hepatocytes and Kupffer cells, mouse livers were perfused through the portal vein with 25 mL of Hanks solution containing 2.5 mM EGTA at 37°C at a rate of 20 mL per 5 minutes. Next, 100 mL of buffer containing 0.05% collagenase was recirculated at a rate of 20 mL per 5 minutes through the liver for

approximately 18 minutes. Then, livers were cut into approximately 1-mm³ pieces and incubated with 0.1% type IV collagenase at 37°C for 30 minutes for further digestion. The incubation cocktail was blown gently with a pipette to help cell dispersion. The cell suspension was filtered through a 75-μm cell strainer, and the filtrate was centrifuged and resuspended in DMEM supplemented with 10% FBS and 1% penicillin-streptomycin. Cells (1 × 10⁶ per well) were plated in 6-well plates in DMEM supplemented with 10% FBS and 20 mM HEPES. Cells reached confluence in 2 days and then were either incubated with [³H]OA or transfected to overexpress or knock down genes of interest. Isolated Kupffer cells were placed in DMEM with 10% FBS plus 25% L cell–conditioned medium (17).

Uptake of fatty acids by cells in culture. Hepatocytes or Kupffer cells from C57BL/6J mice were transfected with *siClk* or *siCtrl* for 48 hours and then incubated with [³H]OA in serum-free DMEM at 37°C for 1 hour. Kupffer cells from different mice were placed in DMEM with 10% FBS for 1 week; then cells were incubated with [³H]OA (0.5 μCi/mL) in FBS-free DMEM at 37°C for 1 hour. Radioactivity in the medium and cells was quantified by scintillation counting. The assays were performed in quadruplicate, and results are presented as percentage uptake (15–17, 31).

Fatty acid oxidation by cells in culture and in liver slices. Fresh liver slices (<10 mg each) were incubated with [¹⁴C]PA (0.2 μCi/mL) or [¹⁴C]OA (0.2 μCi/mL) for 2 hours, and radiolabeled CO_2 was trapped on a filter paper soaked with phenylethylamine. In cells, oxidation was determined by quantification of ¹⁴C-acid-soluble β-oxidation products after 1-hour incubations. Measurements were performed as previously described (41).

Liver fatty acid uptake in vivo. Mice were fasted for 4 hours and injected i.p. with 1 μCi/mouse of [³H]OA in 0.25 mL of PBS. Blood (20 μL) was obtained from the tail vein at different times, and the liver was collected at the end. Plasma and liver pieces were used for liquid scintillation counting. Liver counts were normalized to 1 mg of liver protein.

Tissue preparation and histologic examination. Fresh liver tissues were cut, mixed with OCT compound, rapidly frozen in liquid nitrogen, and stored at –80°C. Frozen sections were cut (6 μm thick) and used for Oil Red O and H&E staining. TUNEL staining was conducted using a kit (Roche). Liver sections were also formalin fixed and paraffin embedded. For immunohistochemistry, fixed tissues were sent to HistoWiz.

Western blot analysis. Liver pieces were homogenized in lysis buffer. Proteins (20 μg/lane) were separated under nonreducing conditions using SDS-PAGE, transferred to nitrocellulose membranes, and blocked for 2 hours in TBS–Tween-20 buffer containing 5% nonfat dry milk at room temperature. The blots were washed 3 times and incubated overnight at 4°C in the same buffer with a primary antibody (1:100 to 1:1000 dilution), washed, and then incubated with mouse HRP-conjugated secondary antibody (1:1000 to 1:4000) in 1.0% nonfat dry milk for 1 hour at room temperature. Immune reactivity was detected by chemiluminescence (15–17, 38).

Quantitative real-time PCR. Liver tissues were stored at –80°C, and total RNA was isolated using Trizol (Invitrogen). Isolated total RNA was reverse-transcribed (15–17, 38) and used for real-time PCR. Primers used are shown in Supplemental Table 3. 18S rRNA was used as the reference gene. The mRNA expression level of Arppo was used as the control (17).

ChIP assay. Liver tissues or primary cells were subjected to ChIP using the ChIP assay kit (USB, catalog 78460) according to the instructions; specific goat polyclonal antibodies used are described in Supplemental Table 1. DNA samples recovered after immunoprecipitation were subjected to PCR using gene-specific primers (Supplemental Table 3), and subjected to agarose gel electrophoresis. For negative controls, ChIP was performed in the absence of antibody or in the presence of rabbit IgG. These experiments were repeated 3–4 times, and similar results were obtained. Data from 1 individual representative experiment are provided.

Lipoprotein production in vivo. Mice (fasted for 5 hours from 10 am) were injected i.p. with 0.5 mL of poloxamer 407 in PBS (1 mg/mouse body weight, 1:6, vol/vol), and blood was collected at different times. Plasma was used for liquid scintillation counting and lipid measurements. Triglyceride synthesis and fatty acid oxidation experiments were performed as previously described (42).

Statistics. Statistical analysis was performed using GraphPad Prism software. Data are presented as means ± SD. Statistical testing was performed using Student's *t* test. Multiple comparisons between groups were performed using 1-way or 2-way ANOVA followed by indicated post-tests (GraphPad Prism). Differences were considered statistically significant when *P* was less than 0.05.

Study approval. Animal protocols were approved by the Animal Care and Use Committees of SUNY Downstate Medical Center and NYU Winthrop Hospital, Mineola, New York, USA.

Author contributions

XP designed and performed experiments, analyzed data, interpreted results, discussed implications, and wrote and critically evaluated the manuscript. MMH supervised the project, interpreted results, discussed implications, obtained funding, and wrote the manuscript. JQ performed cryosectioning and staining of the tissues.

Acknowledgments

Address correspondence to: M. Mahmood Hussain, Department of Foundations of Medicine, New York University Long Island School of Medicine, Research and Academic Building, 101 Mineola Blvd, Suite 3-041, Mineola, New York 11501 USA. Email: Mahmood.hussain@nyulangone.org. Or to: Xiaoyue Pan, Department of Foundations of Medicine, New York University School of Medicine, Research and Academic Center, 101 Mineola Blvd, Suite 4-002, Mineola, New York 11501, USA. Email: xiaoyue.pan@nyulangone.org.

1. Diehl AM, Day C. Cause, pathogenesis, and treatment of nonalcoholic steatohepatitis. *N Engl J Med*. 2017;377(21):2063–2072.
2. Friedman SL, Neuschwander-Tetri BA, Rinella M, Sanyal AJ. Mechanisms of NAFLD development and therapeutic strategies. *Nat Med*. 2018;24(7):908–922.
3. Bessone F, Razori MV, Roma MG. Molecular pathways of nonalcoholic fatty liver disease development and progression. *Cell Mol Life Sci*. 2019;76(1):99–128.
4. Mazzoccoli G, De Cosmo S, Mazza T. The biological clock: a pivotal hub in non-alcoholic fatty liver disease pathogenesis. *Front Physiol*. 2018;9:193.
5. Shetty A, Hsu JW, Manka PP, Syn WK. Role of the circadian clock in the metabolic syndrome and nonalcoholic fatty liver disease. *Dig Dis Sci*. 2018;63(12):3187–3206.
6. Turek FW, et al. Obesity and metabolic syndrome in circadian Clock mutant mice. *Science*. 2005;308(5724):1043–1045.
7. Wang GL, Jiang BH, Rue EA, Semenza GL. Hypoxia-inducible factor 1 is a basic-helix-loop-helix-PAS heterodimer regulated by cellular O2 tension. *Proc Natl Acad Sci U S A*. 1995;92(12):5510–5514.
8. Semenza GL. HIF-1 mediates metabolic responses to intratumoral hypoxia and oncogenic mutations. *J Clin Invest*. 2013;123(9):3664–3671.
9. Schito L, Semenza GL. Hypoxia-inducible factors: master regulators of cancer progression. *Trends Cancer*. 2016;2(12):758–770.
10. Koivunen P, Kietzmann T. Hypoxia-inducible factor prolyl 4-hydroxylases and metabolism. *Trends Mol Med*. 2018;24(12):1021–1035.
11. Fong GH, Takeda K. Role and regulation of prolyl hydroxylase domain proteins. *Cell Death Differ*. 2008;15(4):635–641.
12. Wu Y, et al. Reciprocal regulation between the circadian clock and hypoxia signaling at the genome level in mammals. *Cell Metab*. 2017;25(1):73–85.
13. Hogenesch JB, Gu YZ, Jain S, Bradfield CA. The basic-helix-loop-helix-PAS orphan MOP3 forms transcriptionally active complexes with circadian and hypoxia factors. *Proc Natl Acad Sci U S A*. 1998;95(10):5474–5479.
14. Peek CB, et al. Circadian clock interaction with HIF1α mediates oxygenic metabolism and anaerobic glycolysis in skeletal muscle. *Cell Metab*. 2017;25(1):86–92.
15. Pan X, Jiang XC, Hussain MM. Impaired cholesterol metabolism and enhanced atherosclerosis in clock mutant mice. *Circulation*. 2013;128(16):1758–1769.
16. Pan X, Zhang Y, Wang L, Hussain MM. Diurnal regulation of MTP and plasma triglyceride by CLOCK is mediated by SHP. *Cell Metab*. 2010;12(2):174–186.
17. Pan X, Bradfield CA, Hussain MM. Global and hepatocyte-specific ablation of Bmal1 induces hyperlipidaemia and enhances atherosclerosis. *Nat Commun*. 2016;7:13011.
18. Mwaikambo BR, Yang C, Chemtob S, Hardy P. Hypoxia up-regulates CD36 expression and function via hypoxia-inducible factor-1- and phosphatidylinositol 3-kinase-dependent mechanisms. *J Biol Chem*. 2009;284(39):26695–26707.
19. Crucet M, Wüst SJ, Spielmann P, Lüscher TF, Wenger RH, Matter CM. Hypoxia enhances lipid uptake in macrophages: role of the scavenger receptors Lox1, SRA, and CD36. *Atherosclerosis*.
2013;229(1):110–117.
20. Ortiz-Masià D, et al. Induction of CD36 and thrombospondin-1 in macrophages by hypoxia-inducible factor 1 and its relevance in the inflammatory process. *PLoS One*. 2012;7(10):e48535.
21. Koike N, et al. Transcriptional architecture and chromatin landscape of the core circadian clock in mammals. *Science*. 2012;338(6105):349–354.
22. Pizarro A, Hayer K, Lahens NF, Hogenesch JB. CircaDB: a database of mammalian circadian gene expression profiles. *Nucleic Acids Res*. 2013;41(Database issue):D1009–D1013.
23. Li S, et al. CGDB: a database of circadian genes in eukaryotes. *Nucleic Acids Res*. 2017;45(D1):D397–D403.
24. Hirota K, Semenza GL. Regulation of hypoxia-inducible factor 1 by prolyl and asparaginyl hydroxylases. *Biochem Biophys Res Commun*. 2005;338(1):610–616.
25. Koyasu S, Kobayashi M, Goto Y, Hiraoka M, Harada H. Regulatory mechanisms of hypoxia-inducible factor 1 activity: two decades of knowledge. *Cancer Sci*. 2018;109(3):560–571.
26. Ayrapetov MK, et al. Activation of Hif1α by the prolylhydroxylase inhibitor dimethyoxalylglycine decreases radiosensitivity. *PLoS One*. 2011;6(10):e26064.
27. Tous M, Ferré N, Camps J, Riu F, Joven J. Feeding apolipoprotein E-knockout mice with cholesterol and fat enriched diets may be a model of non-alcoholic steatohepatitis. *Mol Cell Biochem*. 2005;268(1–2):53–58.
28. Schierwagen R, et al. Seven weeks of Western diet in apolipoprotein-E-deficient mice induce metabolic syndrome and non-alcoholic steato-

hepatitis with liver fibrosis. *Sci Rep*. 2015;5:12931.

29. Josekutty J, Iqbal J, Iwawaki T, Kohno K, Hussain MM. Microsomal triglyceride transfer protein inhibition induces endoplasmic reticulum stress and increases gene transcription via Ire1α/cJun to enhance plasma ALT/AST. *J Biol Chem*. 2013;288(20):14372–14383.

30. Pan X, Hussain MM. Diurnal regulation of microsomal triglyceride transfer protein and plasma lipid levels. *J Biol Chem*. 2007;282(34):24707–24719.

31. Pan X, Hussain MM. Clock is important for food and circadian regulation of macronutrient absorption in mice. *J Lipid Res*. 2009;50(9):1800–1813.

32. Mesarwi OA, Shin MK, Bevans-Fonti S, Schlesinger C, Shaw J, Polotsky VY. Hepatocyte hypoxia inducible factor-1 mediates the development of liver fibrosis in a mouse model of nonalcoholic fatty liver disease. *PLoS One*. 2016;11(12):e0168572.

33. Semenza GL. Hypoxia-inducible factors in physiology and medicine. *Cell*. 2012;148(3):399–408.

34. Liu Y, et al. HIF-1α and HIF-2α are critically involved in hypoxia-induced lipid accumulation in hepatocytes through reducing PGC-1α-mediated fatty acid β-oxidation. *Toxicol Lett*. 2014;226(2):117–123.

35. Hansen HH, Feigh M, Veidal SS, Rigbolt KT, Vrang N, Fosgerau K. Mouse models of nonalcoholic steatohepatitis in preclinical drug development. *Drug Discov Today*. 2017;22(11):1707–1718.

36. Chen K, Ma J, Jia X, Ai W, Ma Z, Pan Q. Advancing the understanding of NAFLD to hepatocellular carcinoma development: from experimental models to humans. *Biochim Biophys Acta Rev Cancer*. 2019;1871(1):117–125.

37. Zhang D, et al. The hepatic BMAL1/AKT/lipogenesis axis protects against alcoholic liver disease in mice via promoting PPARα pathway. *Hepatology*. 2018;68(3):883–896.

38. Pan X, et al. Circadian regulation of intestinal lipid absorption by apolipoprotein AIV involves forkhead transcription factors A2 and O1 and microsomal triglyceride transfer protein. *J Biol Chem*. 2013;288(28):20464–20476.

39. Kutteh WH, Rainey WE, Carr BR. Glucocorticoids inhibit lipopolysaccharide-induced production of tumor necrosis factor-alpha by human fetal Kupffer cells. *J Clin Endocrinol Metab*. 1991;73(2):296–301.

40. Sunman JA, Hawke RL, LeCluyse EL, Kashuba AD. Kupffer cell-mediated IL-2 suppression of CYP3A activity in human hepatocytes. *Drug Metab Dispos*. 2004;32(3):359–363.

41. Irani S, Pan X, Peck BC, Iqbal J, Sethupathy P, Hussain MM. MicroRNA-30c mimic mitigates hypercholesterolemia and atherosclerosis in mice. *J Biol Chem*. 2016;291(35):18397–18409.

42. Soh J, Iqbal J, Queiroz J, Fernandez-Hernando C, Hussain MM. MicroRNA-30c reduces hyperlipidemia and atherosclerosis in mice by decreasing lipid synthesis and lipoprotein secretion. *Nat Med*. 2013;19(7):892–900.